

Genesis and preservation of authigenic magnetite and greigite in the cold seep sediments, Bay of Bengal

Firoz Badesab^{1*}, Virsen Gaikwad^{1,2}, Mamilla Venkateshwarlu³, Nitin Kadam^{1,2}

¹ CSIR - National Institute of Oceanography, Dona Paula, Goa, India

² School of Earth Ocean and Atmospheric Sciences, Goa University, Goa, India

³ CSIR - National Geophysical Research Institute, Uppal Road, Hyderabad, India

Corresponding author: Firoz Badesab (firoz@nio.org)

Abstract

We report a new mechanism of authigenic greigite and magnetite formation and preservation in an anomalous “sulfide-rich” interval in the cold (methane) seep sediments from the Bay of Bengal. Rock magnetic proxies (SIRM/ χ_{lf} , ARM/SIRM) coupled with microscopic (TEM, SEM) observations provided compelling evidence for the presence of nanoscale authigenic magnetite and greigite particles in the methanic sediments. Multiple peaks of SIRM/ χ_{lf} coupled with high Hcr (>53 mT) and D_{JH} values suggest significant contribution from authigenic greigite particles to the bulk sediment magnetism. High ARM/SIRM in the sulfide-rich intervals within methanic zone suggest that nanoscale authigenic magnetite formation is closely linked with the microbial iron reduction process fuelled by anaerobic oxidation of methane (AOM). We proposed that enrichment of reactive secondary iron (oxyhydr) oxides through selective leaching of Fe²⁺ during diagenetic dissolution and maghemitization of detrital magnetic particles and iron-sulfide mineral oxidation at the paleo-SMTZ fronts, hindered the pyritization processes and favoured microbial iron reduction which led to the formation and preservation of authigenic greigite and magnetite in methanic sediments.

Keywords: Cold Seep, Rock Magnetism, Authigenesis, Magnetic Minerals, Bay of Bengal.

1. Introduction

Marine cold seeps systems are characterized by seepage of fluids enriched in methane and hydrogen sulfide migrating from deep reservoirs to the seafloor (Suess, 2014). Microbial-mediated biogeochemical reactions driving the diagenesis and authigenesis of magnetic minerals at cold seep site depend on the methane and sulfate concentration and sedimentation rates (Canfield and Berner, 1987; Karlin, 1990; Leslie et al., 1990; Liu, 2004; Garming et al., 2005; Rey et al., 2005; Sagnotti et al., 2005; Horng and Chen, 2006; Dewangan et al., 2013; Riedinger et al., 2014; Kars and Kodama 2015; Roberts, 2015; Lin et al., 2017; Amiel et al., 2020; Gaikwad et al., 2021; Ahn et al., 2021; Yang et al., 2022). Authigenesis of magnetic minerals (greigite, magnetite) in marine cold seep system and its impact on bulk sediment magnetism is less well studied than more prevalent steady and non-steady state magnetic mineral diagenesis mainly due to the complex interplay of competing microbiological and geochemical reactions constrained by variable methane and sulfate fluxes (Jiang et al., 2001; Larrasoña et al., 2007; Fu et al., 2008; Dewangan et al., 2013; Kars and Kodama, 2015; Roberts, 2015; Chang et al., 2008, 2016; Liu et al., 2018; Amiel et al., 2020; Gaikwad et al., 2022; Yang et al., 2022). Mechanism of ferrimagnetic iron sulfides formation via microbially mediated diagenetic reactions has been well documented in Cascadia Margin, offshore Oregon (Larrasoña et al., 2007), Mamanguá Ría, Brazil (Rodelli et al., 2018, 2019), South Atlantic (Dantas et al., 2022), and Mediterranean Continental Shelf (Amiel et al., 2020). Karlin (1987) described authigenic magnetite formation under suboxic conditions in marine sediments. Kars and Kodama (2015) highlighted linkage between authigenic greigite precipitation and formation in the gas hydrate-bearing sediments in the Nankai Trough, offshore Japan. Phillips et al. (2017) documented a linkage between authigenic formation of magnetite and microbial iron-reduction process in the sediments offshore Shimokita Peninsula, Japan. Lin et al. (2020) reported a novel source driving magnetite authigenesis in gas hydrate bearing intervals from South China Sea. Gaikwad et al. (2022) provided a comprehensive view of the methane-influenced diagenetic and authigenic processes in the deep-seated marine gas hydrate system from the Bay of Bengal. Yang et al. (2022) explained how multiple turbiditic and bioturbated intervals modulated the mechanism of greigite formation and preservation in the deep sea sediments Offshore Sumatra. However, a dedicated study aimed at understanding the genesis of magnetic minerals and their state of preservation linked with microbial-mediated geochemical reactions in sulfidic and methanic environment was still lacking.

A sediment (gravity) core collected from the cold seep site in the Bay of Bengal during Council of Scientific and Industrial Research (CSIR)-National Institute of Oceanography (NIO) gas hydrate discovery cruise (SSD-045 onboard R/V Sindhu Sadhana; Mazumdar et al., 2019) provided an

excellent opportunity to elucidate the mechanism controlling the authigenesis of greigite and magnetite in the methanic sediments. In this study, we report the existence of high magnetic susceptibility, coercivity, and ferrimagnetic grain size linked with the presence of nanoscale authigenic magnetite and greigite particles in an anomalous “sulfide-rich” interval at the cold seep site in the Bay of Bengal (Chang et al., 2009; Peketi et al., 2022). We evaluated rock magnetic, mineralogical, and microscopy data of the sediment core (SSD-045/Stn-4/GC-04) from the marine cold seep system to unravel the mechanism of greigite and magnetite authigenesis linked with AOM coupled microbial iron-reduction processes in an anomalous “sulfide-rich” sedimentary intervals.

2. Geological Setting

The Krishna-Godavari (K-G) basin is a pericratonic, petroliferous rift basin situated in the central part of the eastern continental margin of India (ECMI) (Figure 1). The sediment thicknesses reported from the K-G basin varies from 3 to 5 km in the onshore region and about 8 km in the offshore region (Prabhakar and Zutshi, 1993; Bastia, 2007). The Krishna and Godavari are the major rivers which flows through Late Cretaceous Deccan basalt and late Archaean/early Proterozoic granites and deliver the sediments to the K–G basin (Ramesh and Subramanian 1988; Mukhopadhyay et al., 2010). Annual sediment transport of the Krishna and Godavari rivers is estimated to be around 67.7 and 170×10^6 t, respectively (Biksham and Subramanian, 1988; Ramesh and Subramanian, 1988). Holocene-Pleistocene sedimentary deposits in the K-G basin are dominated by smectite-bearing Godavari clay formations (Rao, 2001). Bulk sediments delivered by the Krishna and Godavari rivers primarily comprised of montmorillonite clay with traces of illite and kaolinite (Subramanian, 1980). Titanomagnetite is the dominant detrital ferrimagnetic mineral present in the K-G basin sediments along with minor amount of titanohematite and largely controlled the magnetic properties of the bulk sediments in terms of its contribution (Sangode et al., 2001, 2007; Dewangan et al., 2013; Kulkarni et al., 2015; Gaikwad et al., 2022). Titanomagnetite is mainly sourced from the Deccan basalts and gets supplied to the K-G basin through the Krishna and Godavari Rivers. Diagenetic dissolution of detrital magnetic minerals and precipitations of secondary authigenic minerals caused by methane-influenced geochemical processes has been well reported in the K-G basin (Usapkar et al., 2014; Badesab et al., 2017, 2019; João et al., 2021; Johnson et al., 2021).

3. Materials and methods

3.1.1. Sediment coring site, sampling and measurements

Gravity core (SSD-045/Stn-4/GC-04) was recovered onboard R/V Sindhu Sadhana (cruise no: SSD-045) from the cold seep location in the K-G basin, Bay of Bengal (Figure 1; Latitude:

15°42.91150'N; Longitude: 82°03.98300'E; water depth: 1805 m; sediment core length: 6.0 m; Peketi et al., 2022). The core was sub-sampled at every 5 cm interval. Dark gray-colored soft sediments in this core yielded a strong odour of hydrogen sulfide after opening the sediment core onboard. Three layers (185 – 190 cmbsf, 190 – 195 cmbsf, and 435 – 440 cmbsf) of light gray colored authigenic carbonates were found in the core (Figure 10).

Sub-sampling of sediment core for magnetic measurements were carried out onboard in the presence of high purity nitrogen flushing to avoid atmospheric conditions, which could otherwise oxidize hydrogen sulfide or iron monosulphide present in the sediments. For rock magnetic analysis, one-hundred and twenty wet sediment samples were weighed, and packed in a 25 mm cylindrical plastic sample bottles. Measurements were carried out at the Paleomagnetic laboratory of CSIR-National Institute of Oceanography (NIO), Goa, India. Specialized rock magnetic measurements including thermomagnetic and hysteresis loop were conducted at the Paleomagnetic Laboratory of CSIR-National Geophysical Research Institute (NGRI), Hyderabad, India.

3.1.2. Rock magnetic analyses

Magnetic susceptibility was measured on the sediment samples at low frequency (0.47 kHz) using a Bartington Instruments MS2B meter, (United Kingdom). Raw volume specific magnetic susceptibility values (κ) were converted to respective mass specific susceptibility (χ) using the calculated density based on known mass of the sample and volume. An anhysteretic remanent magnetization (ARM) was applied in a direct current bias field (50 μ T) in the presence of 100 mT peak alternating field and the remanent magnetization was measured using an AGICO JR-6A automatic spinner magnetometer (Advanced Geoscience Instruments Company), Czech Republic. An isothermal remanent magnetization (IRM) was applied in an inducing field of +2.5T in the forward direction and was demagnetized by DC backfields at -20, -30, -100, and -300 mT using a MMPM10 pulse magnetizer (Magnetic Measurements, United Kingdom). The respective remanences were measured using AGICO JR-6A automatic spinner magnetometer. Mass-normalized IRM acquired at a peak field of 2.5T is considered to be the saturation IRM (SIRM). S-ratio is calculated as the ratio between the IRM at -300 mT and SIRM ($IRM_{-300mT}/SIRM_{2.5T}$; Bloemendal et al., 1992). This ratio indicates the relative proportion of high coercivity compared to soft ferrimagnetic minerals. L ratio is calculated using the equation $[(SIRM_{2.5T}+IRM_{-300mT})/(SIRM_{2.5T} + IRM_{-100mT})]$ Liu et al., 2007; Liu et al., 2012]. Temperature-dependent magnetization curves and the hysteresis loop analyses were carried out using Advanced Variable Field Translation Balance (AVFTB) from Mag-Instruments UG (haftungsbeschränkt), Germany. The magnetic grain size index D_{JH} (Housen and Musgrave, 1996) is the ratio of two axes in the Day plot, i.e., $(Mrs/Ms)/(Hcr/Hc)$.

3.1.3. Electron microscopy and energy-dispersive X-ray spectroscopy

Magnetic particles were extracted from the bulk sediment following Petersen et al. (1986). A scanning electron microscope (SEM; JEOL JSM-5800 LV, Japan) captured the images of magnetic particles in a secondary electron imaging mode at energy levels between 15 and 20 keV. An energy dispersive X-ray spectroscopy (EDS) probe attached to the microscope was used to determine the composition of magnetic particles.

The morphology of the finer magnetic particles was examined using a transmission electron microscope (TEM). TEM imaging and EDS analyses was performed on a JEOL JEM-2100 *plus* TEM, Japan (run with 200 kV acceleration voltages) housed at the sophisticated analytical instrument facility (SAIF), Shivaji University, Kolhapur, Maharashtra, India. The extracted magnetic particles were dispersed in methanol and ultrasonicated for fifteen minutes to get the particles in the suspension. A small drop of the extracted magnetic particles was pipetted onto the copper TEM grid and the methanol was later allowed to evaporate. To minimize the oxidation of magnetic particles, samples were stored in the vacuum desiccator. The elemental composition of the components were determined by energy dispersive x-ray spectrometry (EDS).

3.1.4. X-Ray diffraction analysis

The magnetic mineralogy of the selected samples from different sediment magnetic zones was determined using a Rigaku X-Ray Diffractometer (Ultima IV, Japan). The samples were run from 15° to 70° of 2θ at 1°/min scan speed using Cu Kα radiation (λ 1.5414 Å).

3.1.5. Bulk sediment grain size measurements

Sediment grain size measurements were performed on a Laser Particle Size Analyzer (Malvern Mastersizer 2000, United Kingdom) at CSIR-NIO. For removal of carbonate content, desalinated sediment samples were pre-treated using dilute HCl (1N). Further, same suspensions were treated with 10% H₂O₂ to remove organic carbon content. The sediment dispersing agent (Na-hexametaphosphate) was added to the suspension before the analyses. Grain size values are presented as volume %.

3.1.6. Methane-related authigenic carbonates

Methane-related authigenic carbonates (AGC) were hand-picked during sub-sampling of the sediment core. These materials were washed and cleaned using a distilled water, and later dried at room temperature and stored in the plastic container.

4. Results

4.1. Down-core rock magnetic property variations

Based on the down core changes in the magnetic mineral concentration, composition, and granulometry data, we broadly classified the rock magnetic profile of the sediment core SSD-045/Stn-4/GC-04 into three distinct sediment magnetic zones: Z-I (uppermost 200 cmbsf), Z-II (200 – 390 cmbsf), and Z-III (390 – 600 cmbsf). Magnetic proxies (Figures 2a–b) are generally used as a diagnostic for magnetic mineral concentration. In Z-I and Z-II, a trend of systematic decrease in χ_{lf} and SIRM followed by uniformity in their values from 0 to 390 cmbsf indicate down-core reduction in the magnetic mineral concentration (Figures 2a–b). Z-III exhibit higher values of χ_{lf} and SIRM suggesting highest concentration of magnetic minerals in this zone (Figures 2a-b). The beginning of Z-III is marked by a major increase in the magnetite concentration, and we refer this interval as the zone of enhanced magnetic susceptibility (χ_{lf}). Within this zone (Z-III), several sediment layers which showed distinct rise in χ_{lf} , SIRM, SIRM/ χ_{lf} , and S-ratio indicating the dominance of fine-grained (SP-size) ferrimagnetic particles (Figures 2a-e; Tarduno, 1995; Rowan et al., 2009). Variations in S-ratio can be linked to the changes in magnetic mineralogy. S-ratio exhibit wide range in the values from 0.66 to 0.90 throughout the core suggesting the presence of either higher coercivity magnetic mineral (hematite, goethite) or ferrimagnetic magnetic iron sulfides (greigite, pyrrhotite) (Figure 2e) (Peters and Dekkers, 2003; Roberts et al., 2011). L-ratio is indicative of the coercivity, magnetic grain size, and changes in source of antiferromagnetic minerals (Liu et al. 2007; Liu et al., 2012). L-ratio decrease in Z-I reflect the increase input of low coercivity (~ 100 mT) minerals (Figure 2k). Relatively high and near similar pattern of L-ratio in Z-II and Z-III suggest the dominance of hard magnetic fraction (antiferromagnetic ~ 300 mT; Figure 2k).

4.2. Temperature dependant magnetic susceptibility

Thermomagnetic experiments (Figure 3) confirmed that titanomagnetite is the dominant magnetic mineral present in the sediments (Özdemir and Dunlop, 1997). Increase in χ between 326°C and 412 °C can be attributed to the conversion of paramagnetic minerals into magnetite during heating process (Hirt et al., 1993; Passier et al., 2001; Philips, 2018; Figures 3a–j). Minor peaks between ~ 450 to 500°C (Figures 3a, e, h, j) imply the presence of new magnetic (ferri) phase formed by alteration of pyrite or Fe-bearing clay minerals (Passier et al., 2001).

4.3. Hysteresis loops and Day-Dunlop plot

The hysteresis loops showed characteristic differences in the remanence and coercivity ratios (Figure 4). The remanence ratio (M_{rs}/M_s) of the samples did not vary significantly (0.27-0.35) indicating

less pronounced changes in the magnetic grain size. However, magnetic coercivity ratio (H_{cr} / H_c) showed two-to-three-fold variations (1.92 - 6.33). Wide and narrow shape distribution of the hysteresis curves revealed mixed size magnetic grains. The pot-bellied form of the hysteresis curves indicates the presence of single domain (SD), pseudo-single domain (PSD), and multi-domain (MD) type magnetic grains. Comparatively, Z-II samples showed higher coercivity ratios than other sediment samples (Figures 4c-f). Z-II sample (300 cmbsf; Figure 4e) showed constricted hysteresis loop and very high values of coercivity ratio, which suggests the presence of coarse (MD) magnetic minerals. Lowest values of coercivity ratio were found associated with the sample from Z-III (550 cmbsf; Figure 4i) implying the presence of SD magnetic grains (Dunlop, 2002). Majority of the sediment samples fall in the SP-SD mixing field of the Day-Dunlop plot (Figure 9h), indicating a mixture of fine magnetic particles ranging in size from SP to SD. Mixing of SD with MD grains is also evident in one sample as it falls within PSD field (Figure 9h).

4.4. Scanning electron microscope (SEM)–energy dispersive X-ray spectroscopy (EDS) observations of magnetic particles

SEM-EDS data (Figure 5) confirms and support the interpretation on the magnetic mineralogy in core SSD-045/Stn-4/GC-04. Detrital origin ferrimagnetic iron oxides (titanomagnetite) of various sizes and shapes are found in all magnetic zones (Figure 5). Z-II contain well-preserved titanomagnetite grains. EDS data for these grains indicate the presence of titanium, iron, and oxygen with minor amounts of silicon, aluminium, and magnesium (Figure 5). Diagenetically formed iron sulfides are found to occur as submicron, spherical-shaped particles in all three zones (Figure 5), and EDS spectra contain Fe and S peaks. Authigenic greigite particles occur as bright spots throughout the core. Sub-micron sized iron sulfide particles were also seen to occur as overgrowth on the large titanomagnetite grain in all zones (Figures 5). Presence of such particles in the magnetic extracts from the zone of enhanced χ_{lf} (Z-III) suggest that a ferrimagnetic iron sulfide i.e., greigite or pyrrhotite is the major constituent of the particles occurring as overgrowth on the paramagnetic host substrate such as pyrite (Rowan and Roberts, 2006).

4.5. Transmission electron microscopy (TEM)

TEM observations (Figure 6) on magnetic minerals revealed diverse shapes and sizes of magnetic crystals. We identified isolated magnetofossils of three distinct morphologies: equant, elongated, and bullet-shaped (Figure 6a). The dimensions of these grains ranged from 10 to 50 nm. The morphology and sizes of these magnetic particles are characteristic of magnetofossils. Energy dispersive spectra revealed the chemical composition of magnetic minerals. The presence of iron and

sulphur peaks in the EDS data indicated the presence of abundant magnetite and greigite crystals (Figures 6a-c).

4.6. X-ray diffraction (XRD) analyses of magnetic particles

XRD analyses of extracted magnetic particles from ten representative sediment samples exhibiting wide range in magnetic susceptibility values provided information on different magnetic mineralogies present in all three sediment magnetic zones. Magnetic mineralogy is dominated by titanomagnetite, greigite, and pyrite particles occurring in varying proportion (Figure 7). XRD data confirmed the dominant presence of titanomagnetite along with minor peaks of greigite and pyrite in all three zones (Figure 7). Magnetically enhanced zone (Z-3) contains titanomagnetite, greigite, and pyrite (Figure 7h-j). XRD peaks corresponding to quartz are seen in all the samples (Figure 7).

4.7. Grain size distribution and methane-related authigenic carbonates

Grain size record showed multi-modal type distributions. Bulk sediment grain size in the core SSD-045/Stn-4/GC-04 is dominated by the sand, silt, and clay sized fractions (Figure 10). Sand, silt, and clay content in this core varied from 0.12 to 2.12 vol%, 12.42 to 54.74 vol%, and 39.17–78.22 vol%, respectively. Median grain ranges between 1.22 μm to 7.81 μm (Figure 8a). Sediments in Z-I and Z-II are relatively coarse, while Z-III is marked by very fine-grain size ($< 3 \mu\text{m}$; Figure 8a). Gray color authigenic carbonates of various sizes and morphologies are found only in Z-I and Z-III only (Figure 10).

5. Discussion

5.1. Magnetite authigenesis

Detrital (titanomagnetite, titanohematite), diagenetic (pyrite), and authigenic (magnetite, greigite) magnetic minerals are present in the sediment core SSD-045/Stn-4/GC-04 as confirmed by rock magnetism (Figures 2-4), microscopy (TEM, SEM; Figures 5-6), and XRD data (Figure 7). Based on the sediment pore fluid compositions (Peketi et al., 2022) and observed downcore changes in the magnetic susceptibility (χ) profile, we have demarcated entire sediment rock magnetic record of core into uppermost sulfidic (Z-I, Z-II) and lower most methanic (Z-III) zones (Figure 2). Magnetic grain size proxy (ARM/SIRM) has been successfully used an indicator to detect the presence of fine-grained authigenic magnetite in methanic sediments (Dillon and Bleil, 2006; Lin et al., 2020; Gaikwad et al., 2022). Magnetite authigenesis in methanic sediments has been well-documented and stable SP and SD-type authigenic magnetite formed via AOM processes in the methanic sediments is widely reported (Amiel et al., 2020; Lin et al., 2020; Gaikwad et al., 2022). For example, higher

values of ARM/SIRM linked with magnetite authigenesis in the methanic sediments have been reported from Mediterranean continental shelf (Amiel et al., 2020), Bay of Bengal (Gaikwad et al., 2022), South China Sea (Lin et al., 2020), and offshore Japan (Phillips et al., 2017). In general, two noticeable trends in ARM/SIRM profile are evident in core SSD-045/Stn-4/GC-04. Relatively low and uniform values of ARM/SIRM in the uppermost sulfidic zones (Z-I, Z-II) can be manifested with the selective dissolution of fine-grained magnetic (detrital) particles (Figure 2c). Egger et al. (2015) noticed that abundant iron oxides in the methanogenic region below SMTZ in Bothnian Sea sediments indicating iron reduction. Laboratory based incubations studies of methanic sediments revealed that insitu microbial community bears the potential to link methane oxidation to iron oxide reduction (Boetius et al., 2000; Treude et al., 2014; Riedinger et al., 2014; Aromokeye et al., 2020). In methanic zone (Z-III), elevated ARM/SIRM values can be very well linked to authigenic magnetite formed via microbial iron-reduction process (Phillips et al., 2017; Vigderovich et al., 2019; Lin et al., 2020; Gaikwad et al., 2022). This interpretation is supported by the observed trend of rapid rise in ARM/SIRM below SMTZ in Z-III linked to enhancement in the growth of authigenic (SP, SD) magnetite due to microbial activity driven by iron-reduction process in the methanic zone (Figure 2c; Elmore et al., 1987; Lovely et al., 1987; Phillips et al., 2017; Rodelli et al., 2019; Lin et al., 2020; Gaikwad et al., 2021, 2022). Compared to Z-I and Z-II, a substantial increase in χ_{if} within Z-III (Figure 2a) can be directly attributed to the dominant presence of ferrimagnetic authigenic magnetite and greigite rather than a rapid increase in the concentration of detrital titanomagnetites.

SEM-EDS (Figure 5) and TEM-EDS (Figure 6) observations of magnetic particles provided compelling evidence for the presence of authigenic magnetite and greigite particles of variable size and distinct morphology in the studied sediments. Presence of methane-derived authigenic carbonates (Figure 10) in the core SSD-045/Stn-4/GC-04 imply the existence of suitable geochemical environment, where microbial-mediated iron reduction processes fuelled by AOM is an important metabolic pathway during burial and degradation of organic carbon. Presence of microbial cells in the subsurface layers of the authigenic carbonate samples of biogenic origin from the cold seep sediments in the K-G basin has been well-documented by Sangodkar et al. (2022). This finding suggest that Fe (II) produced by dissimilatory iron reducing bacteria in addition to enrichment of secondary iron (oxyhydr) oxides (via diagenetic dissolution and maghemitization of detrital magnetic particles) in the sediment core SSD-045/Stn-4/GC-04 (present study) was readily available for microbial-mediated authigenesis driving the magnetite formation in Z-III. Magnetic fining trend (Figure 2c) manifested by high χ_{if} (Figure 2a) in the bottommost intervals (495 to 600 cmbsf) within Z-III can be very well associated with higher production of ultra-fine magnetic grains during

magnetite reduction processes (Tarduno, 1995; Chang et al., 2016; Phillips et al., 2017). Relatively lower χ_{lf} values and near-uniform trend of ARM/SIRM in Z-I and Z-II of core SSD-045/Stn-4/GC-04 (Figures 2a,c) can be attributed to lower rate in the production of authigenic magnetite. Such scenario is most likely created either due to reduction in the diffusive methane fluxes because of hydrate accumulation in deeper sediments at this site or newly formed authigenic magnetite during AOM processes might have got selectively dissolved due to intense diagenesis in Z-I and Z-II.

5.2. Greigite authigenesis

Authigenesis of magnetic minerals linked with methane seepage and gas hydrate dynamics support the growth of iron sulfides which imprints new magnetic signals in the host sediments (Housen and Musgrave, 1996; Esteban et al., 2008; Dewangan et al., 2013). For example, authigenic greigite formed via methane-influenced biogeochemical processes in the methane-rich sediments can be very well detected using rock magnetic proxies. The genesis and preservation of authigenic greigite is highly dependent on the amount of reactive iron and dissolved sulfide concentration (Kao et al., 2004; Rowan and Roberts, 2006; Larrasoana et al., 2007). A SIRM/ χ_{lf} has been used successfully utilized to detect the presence of authigenic greigite in the gas hydrate bearing sediments in marine system (Housen and Musgrave, 1996; Musgrave, 2006; Dewangan et al., 2013; Kars and Kodama, 2015; Gaikwad et al., 2022). Association between enrichment of fine-grained (SP, SD) size particles and authigenic growth of ferrimagnetic iron sulfides (greigite, pyrrhotite) in the sulfidic and methanic sediments has been well reported (Snowball, 1991; Larrasoana et al., 2007; Rowan et al., 2009; Loughheed et al., 2012; Kars et al., 2021; Reinholdsson et al., 2013). Recent study by Kars et al. (2021) highlighted that increase in D_{JH} values can be attributed to the enhancement in the proportion of single domain (SD) ferrimagnetic (greigite) particles. Multiple peaks of SIRM/ χ_{lf} coupled with high H_{cr} (>53 mT) and D_{JH} values confirmed the widespread occurrence and significant contribution from authigenic (SD) greigite throughout the sediment core. This observations is further supported by microscopy (TEM-EDS, SEM-EDS; Figures 5-6), and XRD (Figure 7) data (Neretin et al., 2004; Larrasoana et al., 2007; Horng, C. S., 2018; Kars et al., 2021). Such scenario points on the variability in diffusive methane flux which unequivocally constrained non-steady-state magnetic mineral diagenesis at this site. We try to investigate how the variability in methane fluxes, microbial activity, and gas hydrate dynamics (formation/dissociation) controlled the genesis and preservation of authigenic greigite intervals in the core SSD-045/Stn-4/GC-04. Changes in the proportion of vertically distributed authigenic greigite particles throughout the core is detected by the presence of multiple greigite peaks in the XRD data (Figure 7), fluctuation in the SIRM/ χ_{lf} (Figure 2d), and H_{cr} (Figure 2g) values. We put forward two plausible explanations. Firstly, increased

rate of pyritization due to intense AOM in Z-I and Z-II probably favored quick conversion of intermediate greigite particles to pyrite as seen through lower peaks in $SIRM/\chi_{lf}$ and χ_{lf} values (Figures 2a, d). Secondly, deficiency of pore water sulfate (Figure 2h) in Z-III might have inhibited the pyritization process (Rowan et al., 2009). Furthermore, higher methane concentration (Figure 2i) coupled with increased availability of reactive iron and low dissolved sulfide concentration enhanced the growth and preservation of authigenic greigite in the methanic zone (Z-III).

Authigenic greigite in marine sediments reported worldwide are mostly in SP or SD state (Roberts, 2015). Magnetic hysteresis derived Day Plot (Figure 9h) and H_{cr} values (53.29 mT to 80.7 mT; Figure 2g) in our samples are similar and falls within the range reported for SP and SD-type authigenic greigite for example, in Hikurangi Margin, New Zealand (Day et al., 1997; Dunlop, 2002; Kars et al., 2021; Reilly et al., 2020; Rowan et al., 2009). This suggests that authigenic greigite in the studied core is mainly dominated by fine size (SP, SD) particles. As seen through SEM-EDS data, numerous overgrowth of sub-micron sized authigenically formed (SP, SD) greigite particles on the larger titanomagnetite grains might have largely contributed to the observed increase in $SIRM/\chi_{lf}$ and χ_{lf} (Figures 2a, d and Figure 5). A trend of gradual decline in S-ratio (Figure 2e) and $SIRM/\chi_{lf}$ (Figure 2d) below SMTZ in Z-III suggest a shift in coercivity of the magnetic particles, as authigenic (SP, SD) greigite particles formed during magnetite reduction processes can also exhibit low S-ratio (Peters and Dekkers, 2003; Dillon and Bleil, 2006; Larrasoña et al., 2007; Kars and Kodama, 2015). Authigenic greigite formed via microbially mediated biogeochemical reactions in the AOM and methane hydrate bearing sediments are reported worldwide (Cragg et al. 1996; Wellsbury et al., 2000; Larrasoña et al., 2007; Blanchet et al., 2009; Rowan et al., 2009; Roberts, 2015; Kars et al., 2021). A close linkage between microbial processes and gas hydrate dynamics (formation/dissociation) has been well-established (Tripathi et al., 2019; Carrier et al., 2020; Kars et al., 2021; Liu et al., 2022). At active marine cold seep system, upward migration of methane through the sediment column and its subsequent oxidation by downward diffusing sulfate could fuel the microbial activity at, near, and below SMTZ. Multiple peaks of high $SIRM/\chi_{lf}$ (Figure 2d) throughout the core also hints on the complex interplay between downward moving sulfate and upward migrating methane fluxes which supported greigite authigenesis (Larrasoña et al., 2007; Dewangan et al., 2013; Kars and Kodama, 2015; Kars et al., 2021). A gradual decrease of $SIRM/\chi_{lf}$ (Figure 2d) below the SMTZ in Z-III can be manifested with the slow conversion of ferrimagnetic greigite to pyrite. Recently Vigderovich et al. (2019) provided molecular and geochemical evidences for microbial iron-reduction in the methanic sediments from Mediterranean Continental shelf. They concluded that iron reduction in the uppermost sulfidic and deeper methanic zone was microbially

mediated. Microbial communities identified at cold seeps in the Krishna-Godavari basin are similar to those reported from cold seep systems worldwide (Sangodkar et al., 2022). Such microorganisms are actively involved in the AOM reaction and control the production of dissolved hydrogen sulfide in the pore waters of host sediments required for the formation of iron sulfides. A dedicated study by Sangodkar et al. (2022) dealing with examination of the microbial and benthic communities associated with the cold seep site in the K-G basin revealed that the microbial associates in the cold seep sediments significantly correlated with methane and hydrogen sulfide concentrations. More recently Kars et al. (2021) highlighted that localized and limited dissolved sulfide generated in situ by AOM processes in the methanic zone support the formation and preservation of authigenic greigite by microbial methanogenesis. Higher SIRM/ χ_{lf} (Figure 2d) and D_{JH} (Figure 2f) values and Day plot (Figure 9h; Day et al., 1977; Dunlop, 2002) in the Z-III indicate the dominant presence of (SP, SD) greigite enhanced by microbial activity in the methanic (Figure 2i) interval of core SSD-045/Stn-4/GC-04.

5.3. Correlation between magnetic and geochemical parameters

A good covariation between χ_{lf} , ARM, and SIRM is observed in majority of the samples, but exhibit differences in their slope suggesting the presence of ferri- and paramagnetic mineral assemblages (Figure 9a-b). A cross plot of SIRM/ χ_{lf} vs. χ_{lf} has been successfully utilized as a proxy for characterizing the magnetic mineral assemblages in the cold seep and gas hydrate bearing sediments (Larrasoana et al., 2007; Kars and Kodama, 2015; Badesab et al., 2019). We broadly classified the samples into three sub groups (Figure 9c). Few samples from Z-III exhibiting higher χ_{lf} and SIRM/ χ_{lf} values suggest the presence of fine-grained authigenically formed greigite particles. Lower values of SIRM/ χ_{lf} and χ_{lf} in the most of samples from Z-I and Z-II (Figure 9c) indicate either increased contribution from paramagnetic iron sulfides relative to ferrimagnetic or lower supply from ferrimagnetic particles (titanomagnetite). Samples from Z-I which lies within the intermediate range of SIRM/ χ_{lf} and χ_{lf} values represent the mixture of magnetic iron sulfides and magnetite (Figure 9c). A plot (χ_{lf} vs ARM/SIRM) diagnostic of authigenic magnetite revealed two distinct groups of ferrimagnetic particles exhibiting fine and coarse-grained magnetic grain sizes. A good covariation between χ_{lf} and mineralogy diagnostic S-ratio is noticed (Figure 9e). Samples from magnetically enhanced zone (Z-III) exhibit two different trends. Samples possessing low S-ratio and relatively narrow range in χ_{lf} can be attributed to the presence of higher coercivity magnetic minerals. Another group of samples from the same zone showed a trend of decrease in S-ratio with increase in χ_{lf} (Figure 9e) and can be attributed to the presence of ferrimagnetic iron sulfides like greigite/pyrrhotite (Figure 9e) (Peters and Dekkers, 2003; Roberts et al., 2011).

5.4. Novel mechanism explaining greigite and magnetite authigenesis in the methanic sediments

Genesis and preservation of greigite and magnetite in methanic sediments is dependent on the amount of available reactive iron, dissolved sulfide concentration, and the sedimentation rate (Garming et al., 2005; Rowan and Roberts, 2006; Larrasoana et al., 2007; Roberts, 2015). In methanic sediments, enrichment of reactive iron and limitation of sulfide concentration created by geochemical processes would favour the authigenic greigite and magnetite formation. In this study, we unravel the mechanism favouring the formation and preservation of authigenic greigite and magnetite in an unprecedented “sulfide-rich” (Figure 2j) interval (Z-III) of core SSD-045/Stn-4/GC-04 which still remained unclear. Rock magnetic, pore-water geochemical, and mineralogical proxies provided convincing evidences of greigite and magnetite authigenesis in the methanic zone (Z-III) of core SSD-045/Stn-4/GC-04. As expected, high methane (Figure 2i) and dissolved hydrogen sulfide (Figure 2j) concentration in Z-III of core SSD-045/Stn-4/GC-04 would readily enhance the pyritization process resulting in complete transformation of metastable greigite to more stable pyrite. Magnetic proxies (SIRM/ χ_{lf} , ARM/SIRM) and Day plot coupled with microscopic (SEM, TEM) observations confirmed the dominance of SP and SD type authigenic greigite and magnetite particles in Z-III. The question remained unanswered was; how does greigite and magnetite formed in sediments rich in dissolved hydrogen sulfide concentration (Figure 2j) and what could be the plausible sources of reactive iron required to drive greigite and magnetite authigenesis? Numerous coarse-grained detrital titanomagnetite and titanohematites particles in Z-III exhibit the signatures of diagenetic dissolution (surficial etching, pits, and lamellae) and maghemitization (shrinkage cracks). We hypothesize that AOM coupled with sulfate-reduction (Figure 2h) released large amount of hydrogen sulfide (Figure 2j) into the surrounding pore-water of host sediments in core SSD-045/Stn-4/GC-04. Preferential leaching of Fe^{2+} out of the abundant Fe-Ti particles during (diagenetic dissolution) and after burial (maghemitization) resulted in the enrichment of reactive iron required for authigenesis of greigite and magnetite in Z-III via microbial iron reduction. χ_{lf} fluctuations within Z-III (Figure 2a) indicated the occurrence of multiple paleo-SMTZ fronts driven by variability in methane seepage (Figure 2i) which resulted in the precipitation of iron sulfides (as confirmed by XRD data; Figure 7) at different sediment depth intervals. Concurrently, oxidation of previously formed iron sulfides via microbial iron-reduction in Z-III (Lin et al., 2020) during low methane seepages also provided adequate supply of secondary iron (oxyhydr) oxides and served as another potential source of iron which is prerequisite for greigite and magnetite authigenesis. We propose that as the concentration of Fe^{2+} overshoot dissolved sulfide level, greigite formation took places in Z-III through alteration of pyritization process (Figure 11). In similar lines, during high seepage

events when such reactive iron oxides (Fe^{2+}) got exposed to methane, microbial iron reduction process led to the formation of authigenic magnetite in Z-III (Lin et al., 2020).

6. Conclusion

We document a new mechanism for greigite and magnetite authigenesis in an unprecedented “sulfide-rich” interval within the methanic sediments from the Bay of Bengal (Figure 11). Enrichment of reactive iron (Fe^{2+}) through selective leaching during diagenetic dissolution and maghemitization of detrital Fe-Ti particles resulted in the arrestation of pyritization processes and favoured microbial iron reduction which led to the formation and preservation of authigenic greigite and magnetite in the methanic sediments. SP and SD-type authigenic greigite and magnetite particles are important magnetic carrier in methanic sediments can survive through geological times and thereby retain the magnetic signal crucial for paleomagnetic studies. Future work integrating microbiology and geochemical study is warranted to elucidate the mechanism through which consortium of AOM coupled microbial iron reduction process and sulfate reducing bacteria constrain the genesis and preservation of authigenic magnetite and greigite in the methanic sediments.

Declaration of competing interest

The authors declare that they have no known competing financial interests or personal relationships that could have appeared to influence the work reported in this paper.

Acknowledgements

Director, CSIR–NIO, Secretary MOES, and National Gas Hydrate Program (NGHP) are thanked for supporting this study. We greatly acknowledge the support of Dr. Aninda Mazumdar, participants of scientific cruise SSD-045 onboard research vessel R/V Sindhu Sadhana of CSIR-NIO, ship cell team (Miliketan Kerkar, Kallathian M, Kuldeep Kumar, and Buddhadas Patole), and ship crews onboard for providing assistance in collection of sediment cores and sampling. We thank the Director of the CSIR-National Geophysical Research Institute (NGRI), Hyderabad, India for providing access to the Paleomagnetic laboratory. Thanks to Girish Prabhu, Areef Sardar, and Prem Piyush Panda for providing assistance with XRD and SEM-EDS analyses at CSIR-NIO. We greatly acknowledge the constructive comments from the associate editor and two anonymous reviewers who helped to improve this manuscript. The data used in this study has been archived at CSIR-NIO data repository and the link to access data online (<https://publication-data.nio.org/s/8dxsdXpHesF4wco>). This is CSIR-NIO publication no. XXXX.

Data availability :The data used in this study has been archived at CSIR-NIO data repository and the link to access data online (<https://publication-data.nio.org/s/8dxsdXpHesF4wco>).

Figures

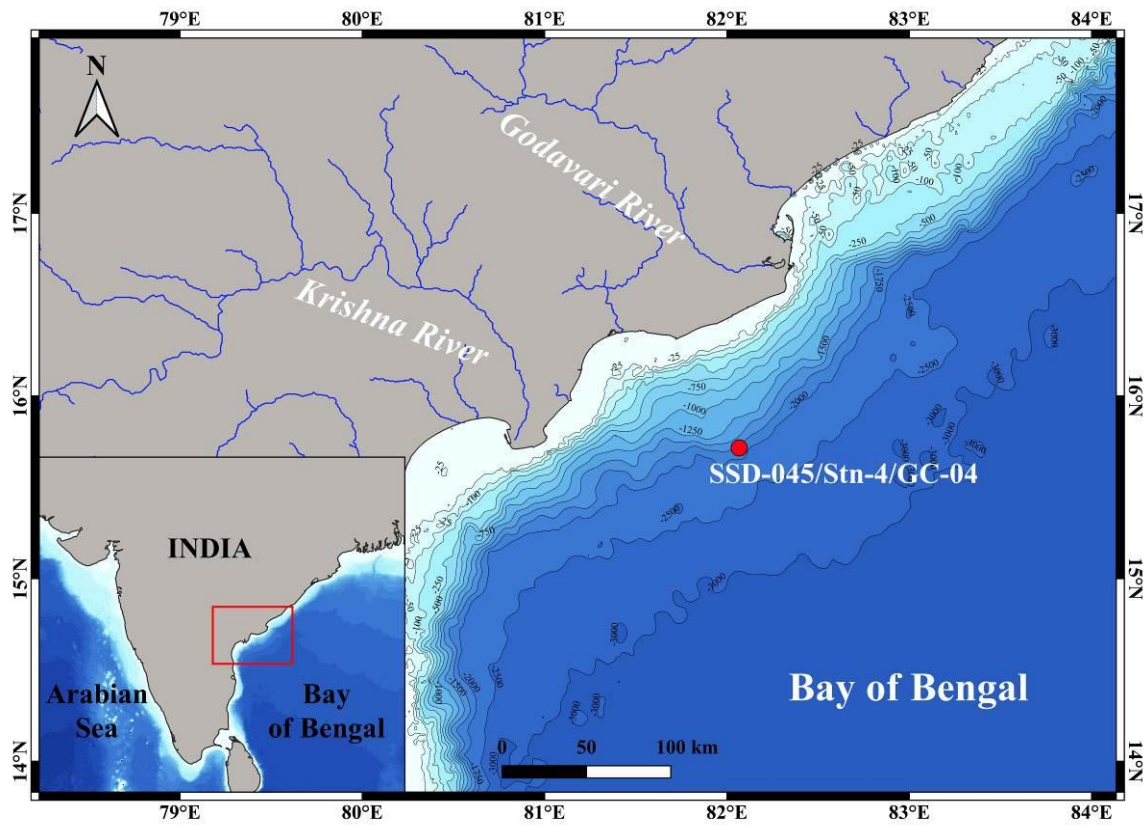


Figure. 1. Map showing the location of sediment core (SSD-045/Stn-4/GC-04; present study) from the cold seep site in the Krishna-Godavari basin, Bay of Bengal (marked by red (filled) circle).

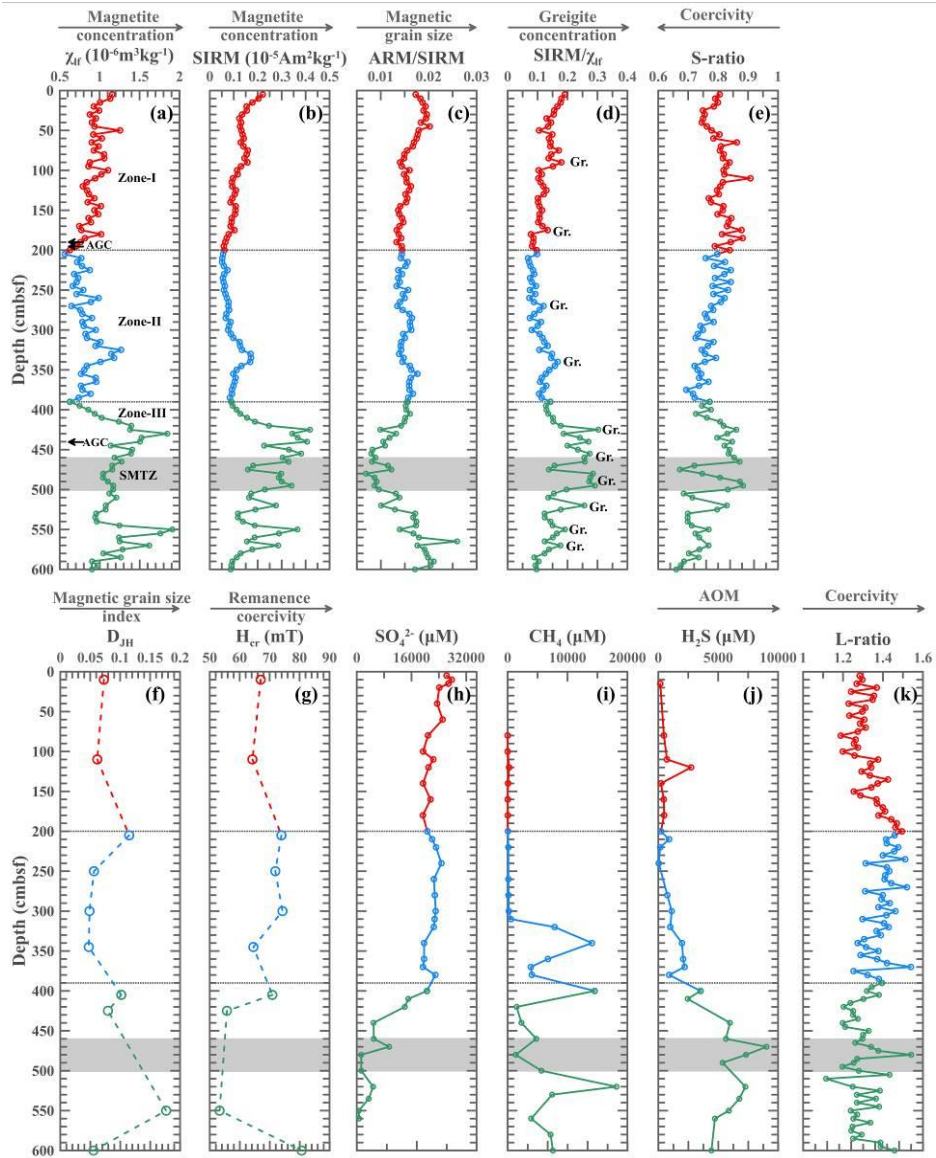


Figure. 2. Depth variations of selected rock magnetic parameters for sediment core SSD-045/Stn-4/GC-04 from the cold seep site in the in the Krishna-Godavari (K-G) basin, Bay of Bengal (a) Magnetic Susceptibility, (b) SIRM, (c), ARM/SIRM, (d) SIRM/ χ_{lf} , (e) S-ratio, (f) magnetic grain size index (D_{JH}), (g) coercivity of remanence (H_{cr}), (h) porewater sulfate (SO_4^{2-}), (i) headspace methane (CH_4) gas concentration, (j) dissolved hydrogen sulfide (H_2S) concentration, and (k) L-ratio. Based on the variation in magnetic susceptibility (χ_{lf}), three sediment magnetic zones (Z-I, Z-II, Z-II) are marked. (Please note that χ_{lf} = low frequency magnetic susceptibility; ARM = anhysteretic remanent magnetization; and SIRM = isothermal remanent magnetization). The arrows (black) on Y-axis indicate the occurrence depth of methane-derived authigenic carbonates in the studied core. The geochemical data of the core SSD-045/Stn-4/GC-04 were taken from the Peketi et al. (2022) (copyright permission obtained). The position of sulphate-methane transition zone (SMTZ) is marked.

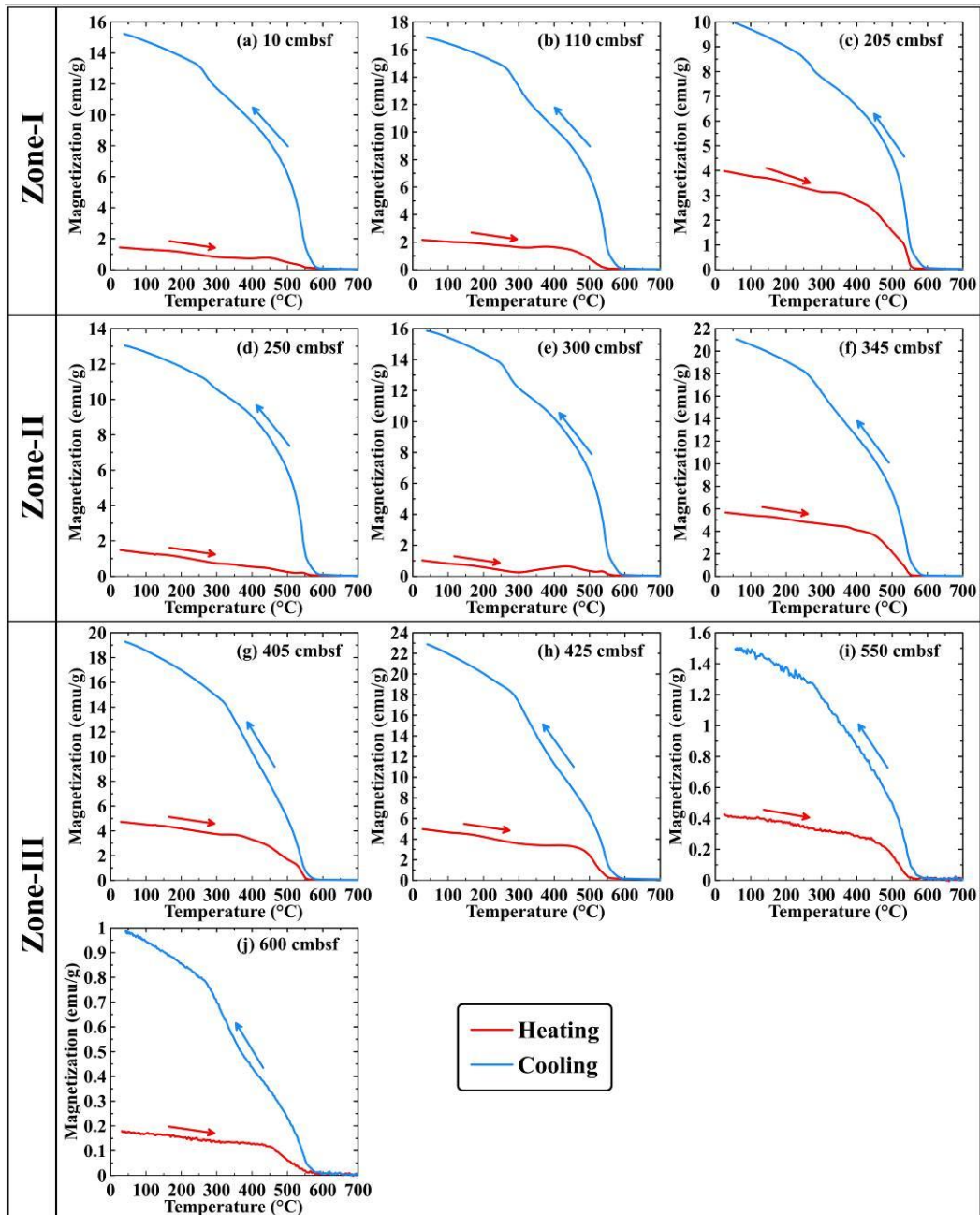


Figure. 3. (a-j) Thermomagnetic heating curves for selected bulk sediment samples from three magnetic zones of sediment core SSD-045/Stn-4/GC-04 from the cold seep location in the Krishna-Godavari (K-G) basin, Bay of Bengal.

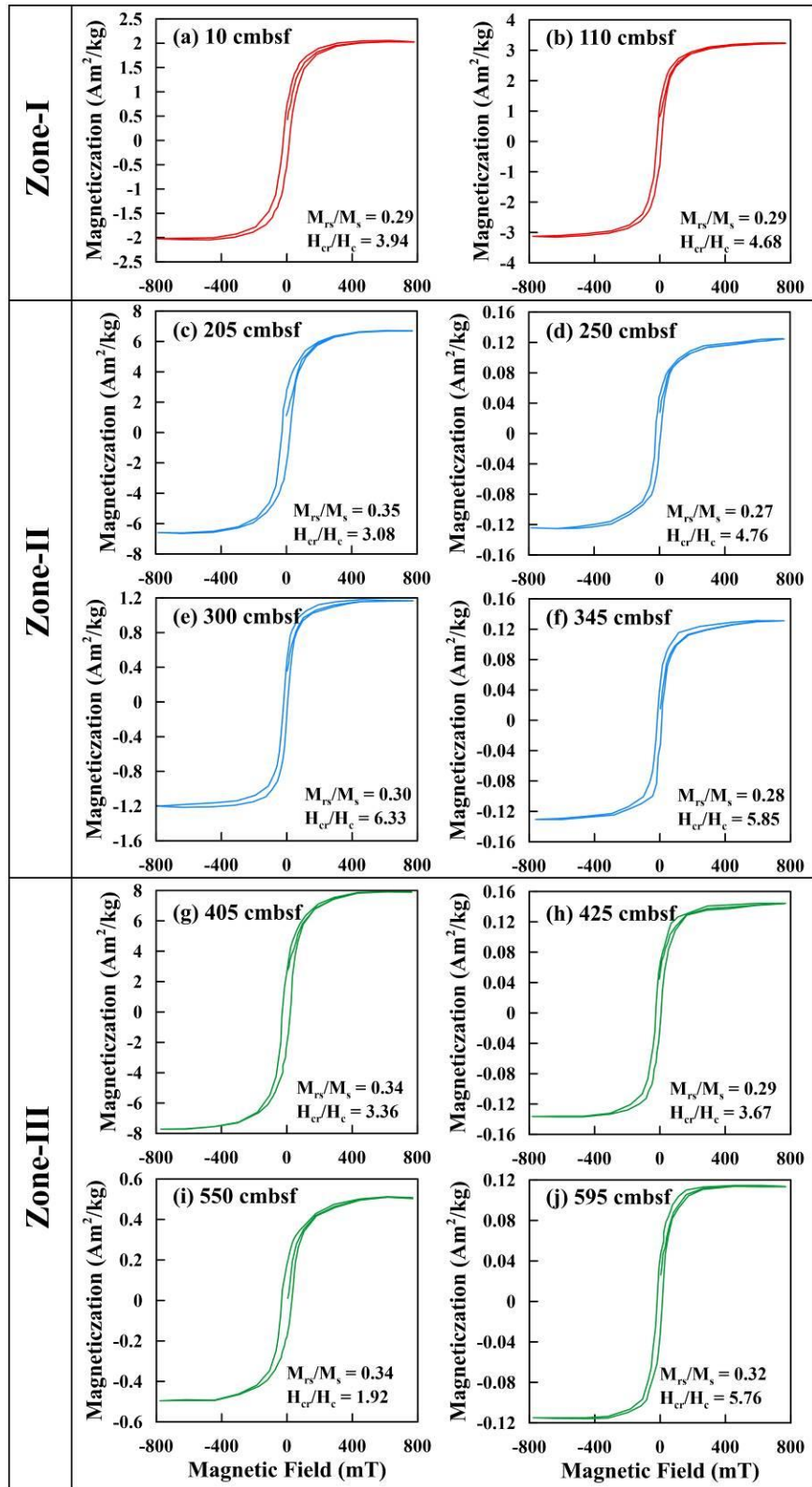


Figure 4. (a-j) Hysteresis loops for selected samples from three magnetic zones (Z-I, Z-II, Z-III) of sediment core SSD-045/Stn-4/GC-04 from the cold seep location in the Krishna-Godavari (K-G) basin, Bay of Bengal. The hysteresis loops have been corrected for the diamagnetic and paramagnetic components.

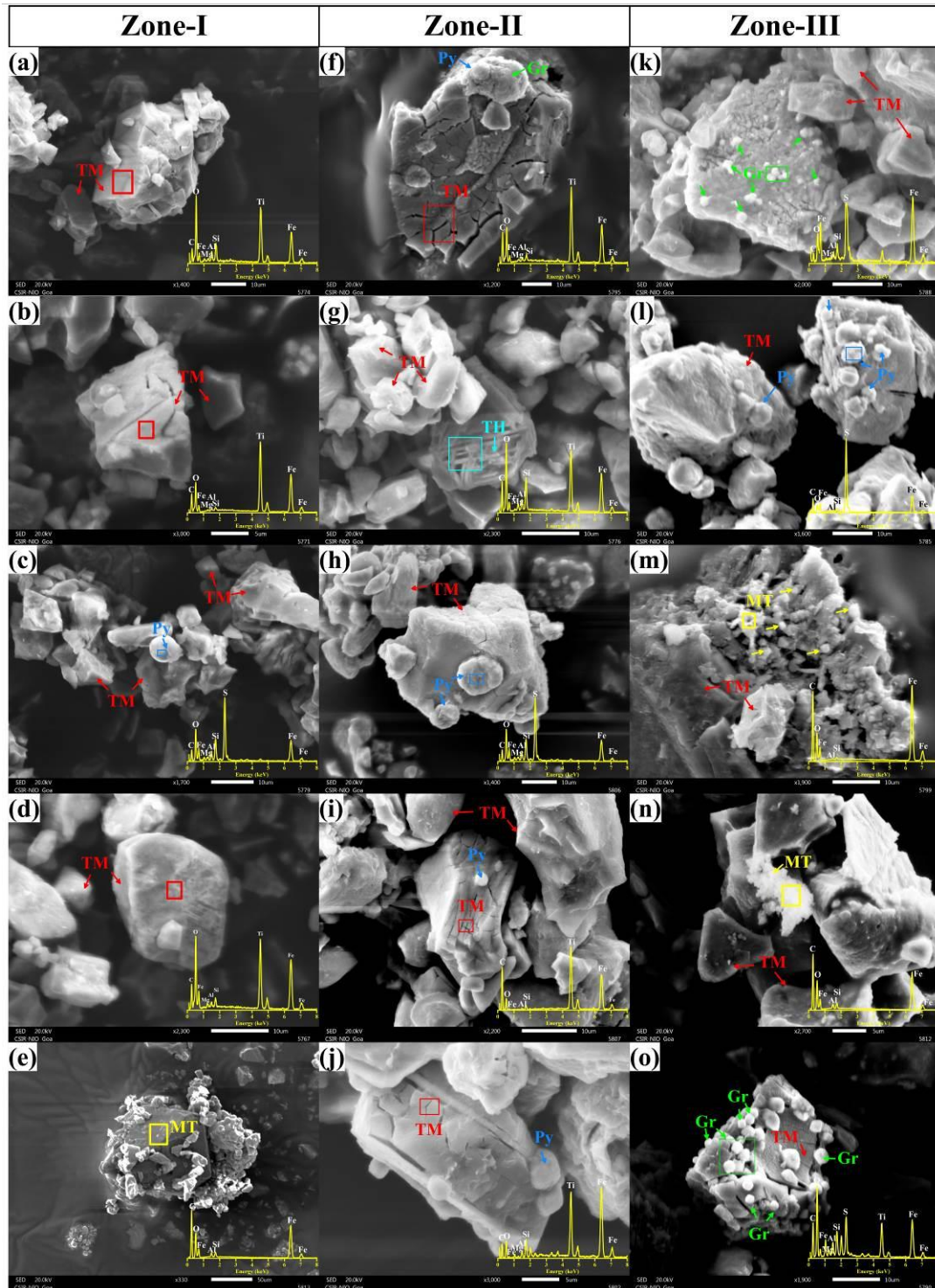


Figure 5. (a-o): Scanning electron microscope (SEM) images on magnetic extracts from three magnetic zones (Z-I, Z-III, Z-III) of core SSD-045/Stn-4/GC-04 from the Krishna-Godavari (K-G) basin, Bay of Bengal. Energy dispersive X-ray spectroscopy (EDS) spectra of the respective images are presented. Iron (Fe), titanium (Ti), sulfur (S), oxygen (O), silicon (Si), carbon (C), aluminium (Al), and magnesium (Mg) peaks are indicated. (TMG: Titanomagnetite, Gr: Greigite, Py: Pyrite, MT: Magnetite, TH: Titanohematite).

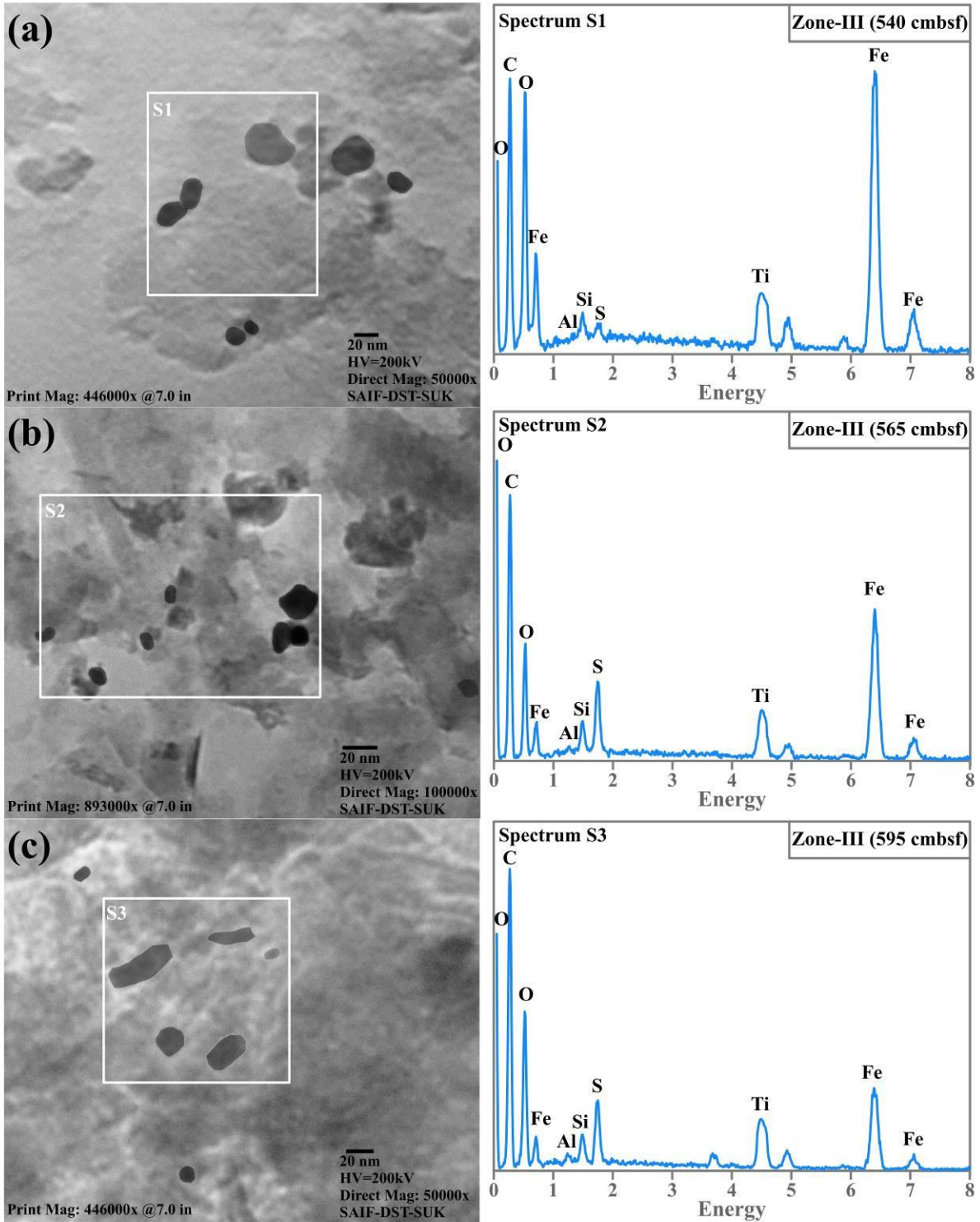


Figure. 6. (a-c): Transmission electron microscope (TEM) images on magnetic extracts from sediment magnetic zone (Z-III) of core SSD-045/Stn-4/GC-04 from the cold seep location in the Krishna-Godavari (K-G) basin, Bay of Bengal. Energy dispersive X-ray spectroscopy (EDS) spectra of the respective images are presented. Iron (Fe), titanium (Ti), sulfur (S), oxygen (O), silicon (Si), carbon (C), and aluminium (Al) peaks are indicated.

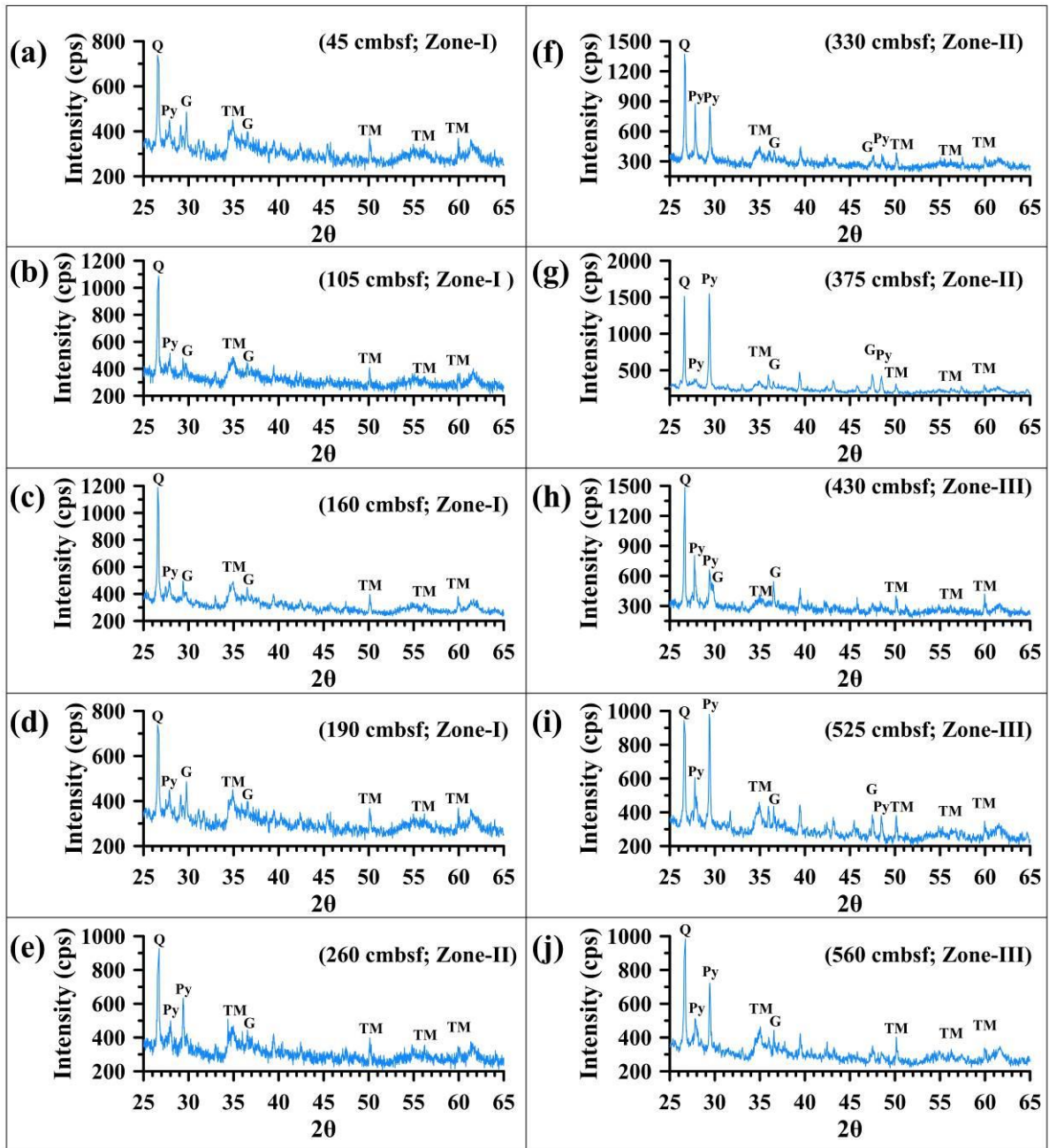


Figure 7. (a-j): X-ray diffraction spectra for extracted minerals from three different sediment magnetic zones (Z-I, Z-II, Z-III) of core SSD-045/Stn-4/GC-04 from the cold seep site in the Krishna-Godavari (K-G) basin, Bay of Bengal. TM = titanomagnetite, G = greigite, Py = pyrite, Q= quartz.

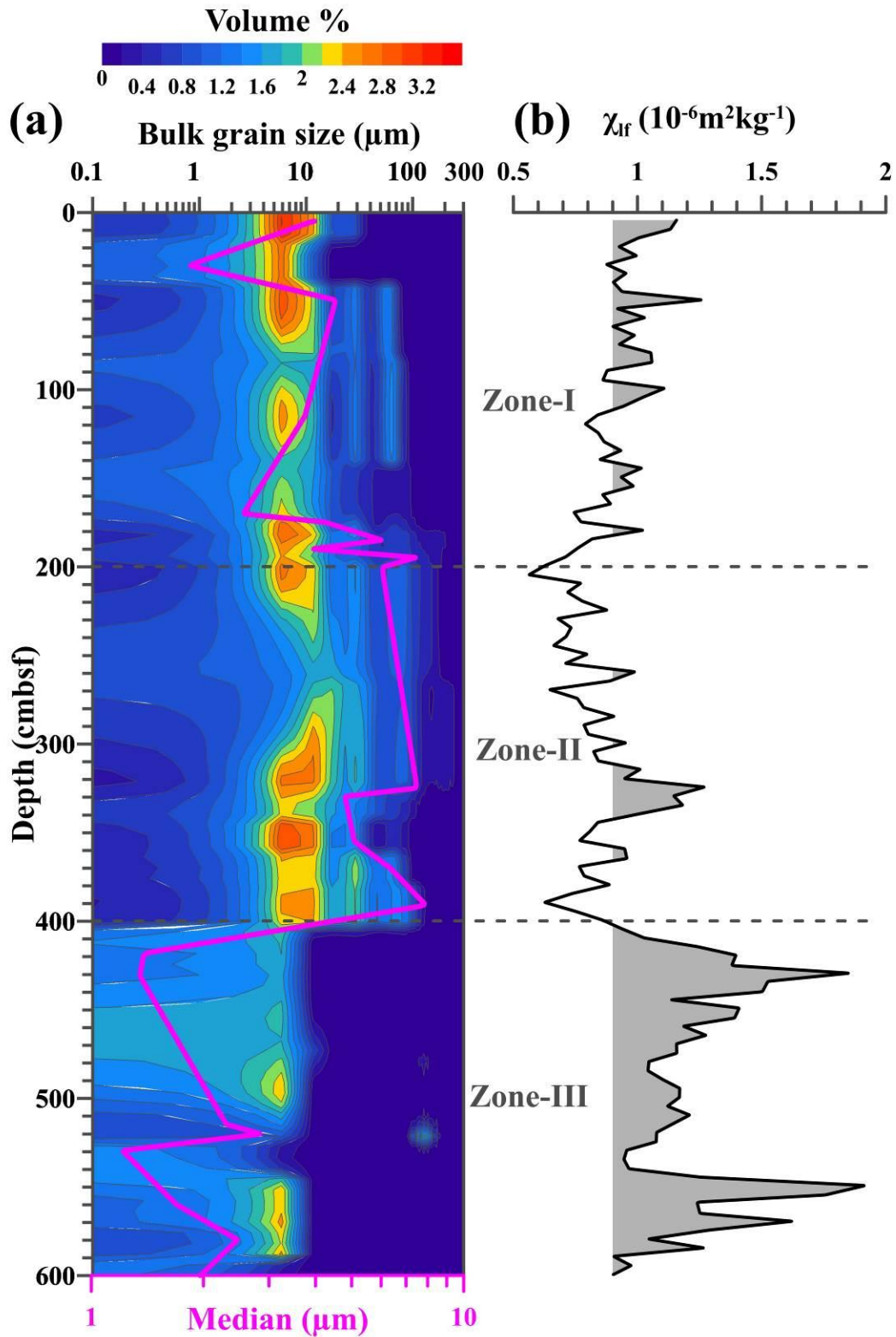


Figure 8. (a) Bulk sediment grain size distribution (vol.%) and median grain size (μm) and (b) magnetic susceptibility of core samples from three different sediment magnetic zones (Z-I, Z-II, Z-III) of sediment core SSD-045/Stn-4/GC-04 from the cold seep location in the Krishna-Godavari (K-G) basin, Bay of Bengal.

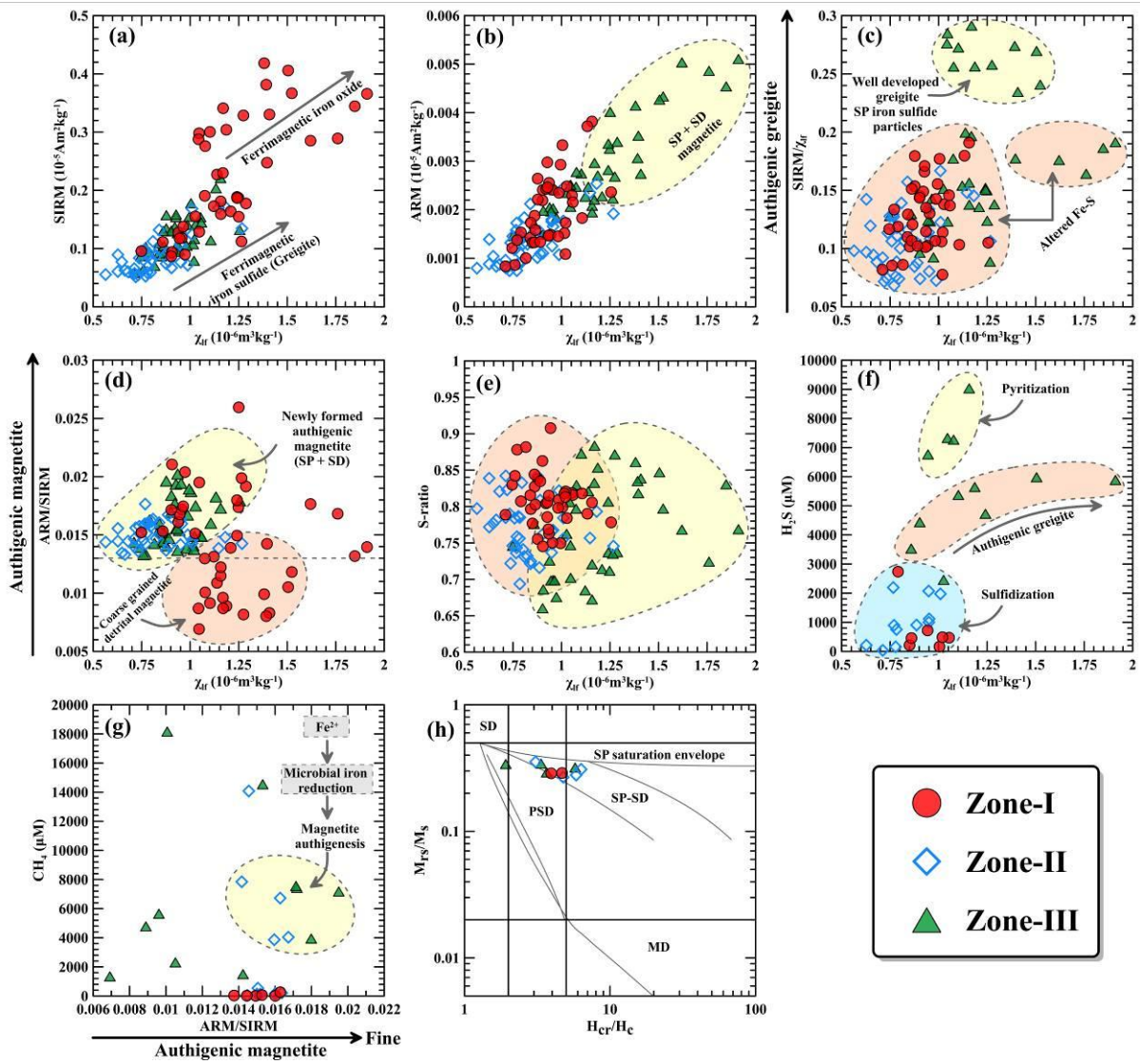


Figure. 9. (a–g): Bivariate scatter plots of rock magnetic and geochemical parameters and (h) Magnetic hysteresis parameters are presented in the Day plot of sediment core SSD-045/Stn-4/GC-04 from the cold seep location in the Krishna-Godavari (K-G) basin, Bay of Bengal.

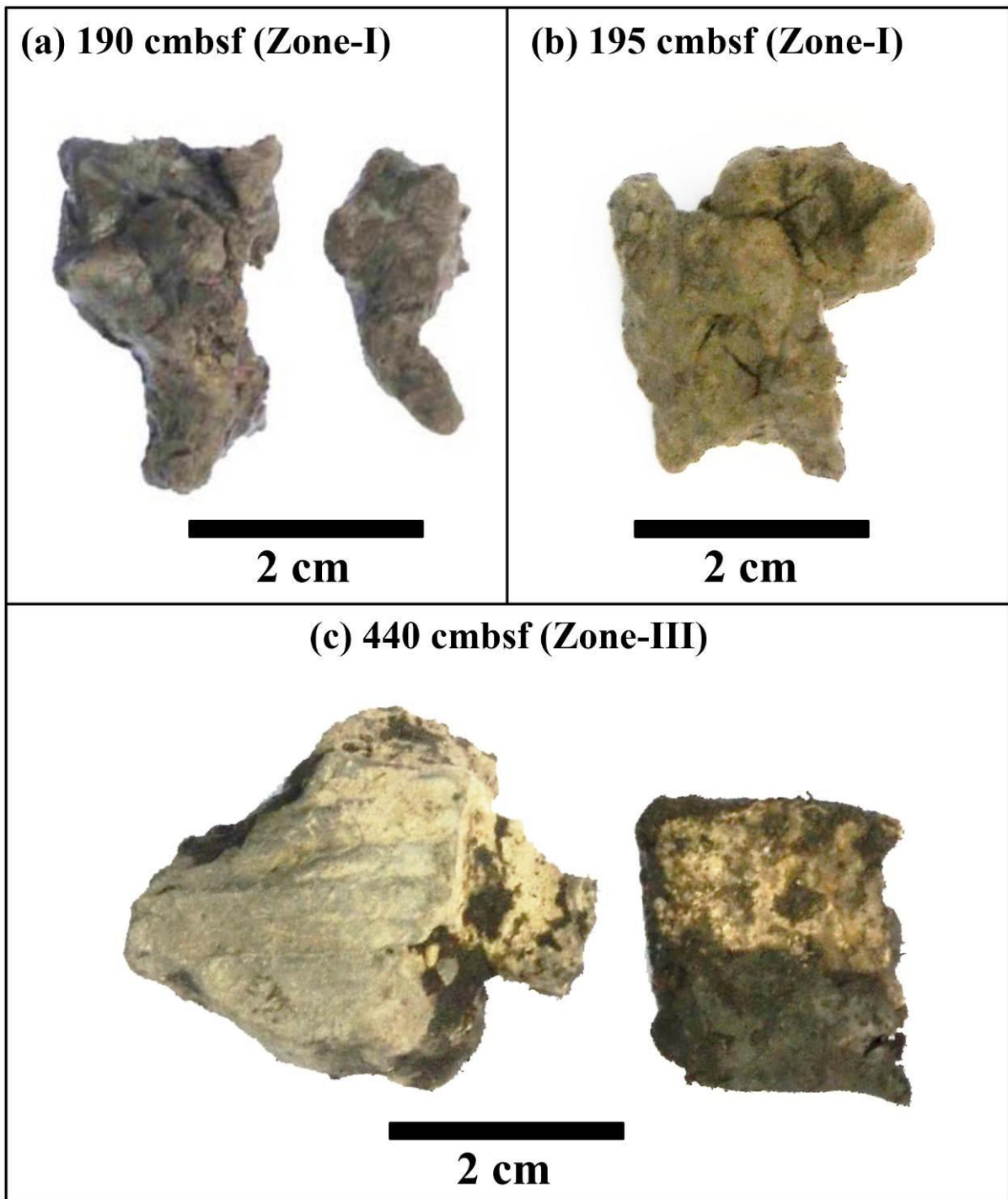
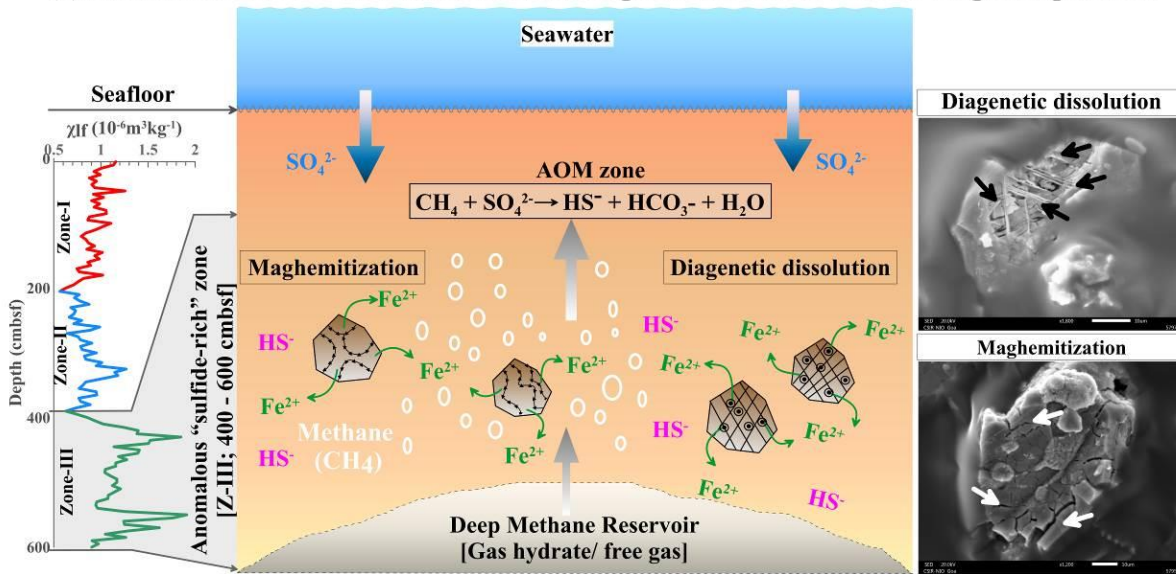


Figure. 10. (a-c) Photographs showing methane-derived authigenic carbonates from different sediment magnetic zones (Z-I, Z-III) of core SSD-045/Stn-4/GC-04 from the cold seep location in the Krishna-Godavari (K-G) basin, Bay of Bengal.

(a) Enrichment of Fe²⁺ via dissolution and maghemitization of detrital magnetic particles



(b) Authigenic greigite and magnetite formation

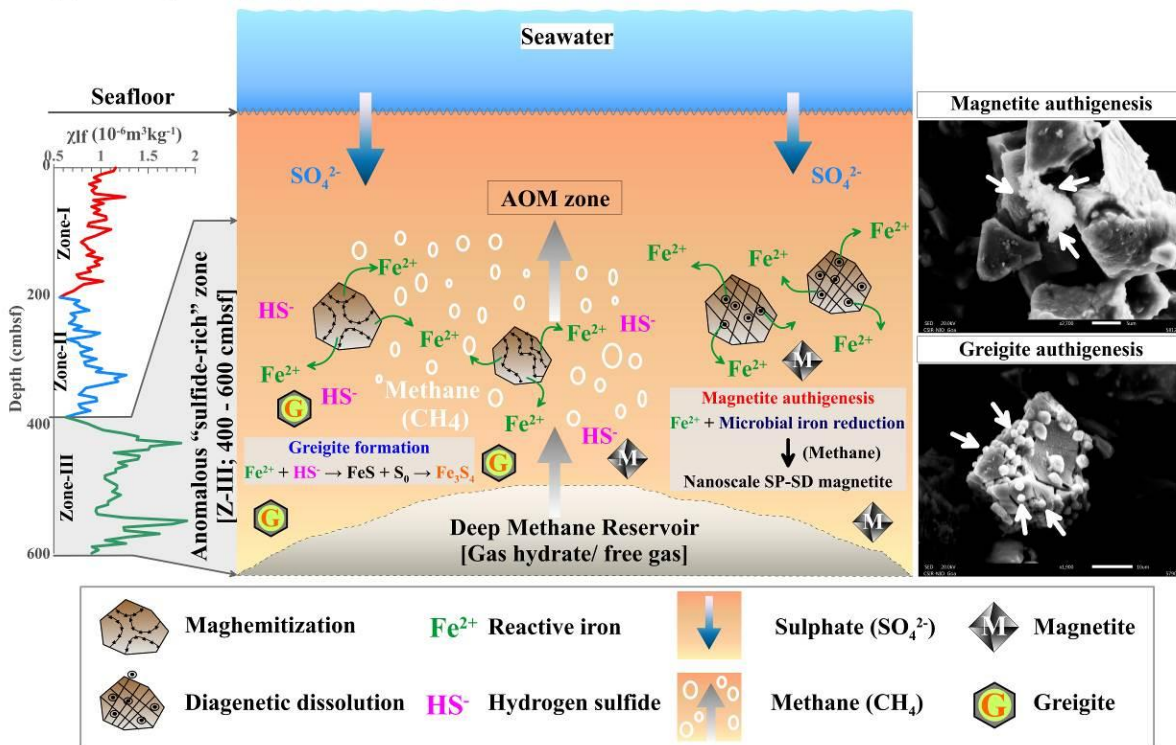


Figure. 11. Conceptual model explaining mechanism of greigite and magnetite authigenesis in the cold seep sediments from the Krishna-Godavari basin, Bay of Bengal.

References

- Aromokeye, D.A., Kulkarni, A.C., Elvert, M., Wegener, G., Henkel, S., Coffinet, S., Eickhorst, T., Oni, O.E., Richter-Heitmann, T., Schnakenberg, A. and Taubner, H., 2020. Rates and microbial players of iron-driven anaerobic oxidation of methane in methanic marine sediments. *Frontiers in Microbiology*, 10, p.3041.
- Ahn H-S., Lim J., and Kim SW., 2021. Magnetic Properties of a Holocene Sediment Core from the Yeongsan Estuary, Southwest Korea: Implications for Diagenetic Effects and Availability as Paleoenvironmental Proxies. *Front. Earth Sci.* 9:593332. doi: 10.3389/feart.2021.593332
- Amiel, N., Shaar, R., Sivan, O., 2020. The Effect of Early Diagenesis in Methanic Sediments on Sedimentary Magnetic Properties: Case Study From the SE Mediterranean Continental Shelf. *Front. Earth Sci.* 8:283. <https://doi.org/10.3389/feart.2020.00283>
- Badesab, F., Dewangan, P., Gaikwad, V., Kars, M., Kocherla, M., Krishna, K.S., et al., 2019. Magnetic mineralogical approach for exploration of gas hydrates in the Bay of Bengal. *J. Geophys. Res. Solid Earth.* 24(5), 4428–4451. <https://doi.org/10.1029/2019JB017466>
- Bastia, R., 2007. Geologic settings and petroleum systems of India's east coast offshore basins: Concepts and applications. Bangalore, India: Technology Publications.
- Biksham, G., Subramanian, V., 1988. Sediment transport of the Godavari River basin and its controlling factors. *Journal of Hydrology*, 101(1-4), 275-290. [https://doi.org/10.1016/0022-1694\(88\)90040-6](https://doi.org/10.1016/0022-1694(88)90040-6)
- Blanchet, C. L., Thouveny, N., Vidal, L., 2009. Formation and preservation of greigite (Fe₃S₄) in sediments from the Santa Barbara Basin: Implications for paleoenvironmental changes during the past 35 ka. *Paleoceanography* 24(2). <https://doi.org/10.1029/2008PA001719>
- Bloemendal, J., King, J.W., Hall, F.R., Doh, S.J., 1992. Rock magnetism of late Neogene and Pleistocene deep-sea sediments: relationship to sediment source, diagenetic processes, and sediment lithology. *J. Geophys. Res. Solid Earth*, 96:4361–4375 <https://doi.org/10.1029/91JB03068>
- Boetius, A., Ravensschlag, K., Schubert, C.J., Rickert, D., Widdel, F., Gieseke, A., Amann, R., Jørgensen, B.B., Witte, U. and Pfannkuche, O., 2000. A marine microbial consortium apparently mediating anaerobic oxidation of methane. *Nature*, 407(6804), pp.623-626.
- Canfield, D. E., Berner, R. A., 1987. Dissolution and pyritization of magnetite in anoxic marine sediments. *Geochim. Cosmochim. Acta.* 51(3), 645–659. [https://doi.org/10.1016/0016-7037\(87\)90076-7](https://doi.org/10.1016/0016-7037(87)90076-7)
- Carrier, V., Svenning, M. M., Gründger, F., Niemann, H., Dessandier, P. A., Panieri, G., Kalenitchenko, D., 2020. The impact of methane on microbial communities at marine arctic gas hydrate bearing sediment. *Frontiers in microbiology*, 11, 1932. <https://doi.org/10.3389/fmicb.2020.01932>
- Chang, L., Roberts, A. P., Tang, Y., Rainford, B. D., Muxworthy, A. R., and Chen, Q., 2008. Fundamental magnetic parameters from pure synthetic greigite (Fe₃S₄). *J. Geophys. Res.* 113:B06104. doi: 10.1029/2007JB005502

- Chang L., Roberts, A. P. Rowan, C. J. Tang, Y. Pruner, P. Chen, Q.-W., and Horng C.-S., 2009. Low-temperature magnetic properties of greigite (Fe₃S₄), *Geochem., Geophys., Geosyst.*, 10, Q01Y04, doi:10.1029/2008GC002276.
- Chang, L., Roberts, A.P., Heslop, D., Hayashida, A., Li, J., Zhao, X. et al., 2016. Widespread occurrence of silicate-hosted magnetic mineral inclusions in marine sediments and their contribution to paleomagnetic recording. *J. Geophys. Res. Solid Earth.* 121(12):8415–8431. <https://doi.org/10.1002/2016JB013109>
- Cragg, B. A., Parkes, R. J., Fry, J. C., Weightman, A. J., Rochelle, P. A., Maxwell, J. R., 1996. Bacterial populations and processes in sediments containing gas hydrates (ODP leg 146: Cascadia Margin). *Earth and Planet. Sci. Lett.* 139, 497–507. [https://doi.org/10.1016/0012-821X\(95\)00246-9](https://doi.org/10.1016/0012-821X(95)00246-9)
- Dantas, R. C., Hassan, M. B., Cruz, F. W., & Jovane, L. 2022. Evidence for methane seepage in South Atlantic from the occurrence of authigenic gypsum and framboidal pyrite in deep-sea sediments. *Marine and Petroleum Geology*, 142, 105727.
- Day R., Fuller M., Schmidt V.A., 1977. Hysteresis properties of titanomagnetites: grain-size and compositional dependence. *Phys. Earth. Planet. Inter.* 13(4):260–267. [https://doi.org/10.1016/0031-9201\(77\)90108-X](https://doi.org/10.1016/0031-9201(77)90108-X)
- Dewangan, P., Basavaiah, N., Badesab, F. K., Usapkar, A., Mazumdar, A., Joshi, R., et al., 2013. Diagenesis of magnetic minerals in a gas hydrate/cold seep environment off the Krishna–Godavari basin, Bay of Bengal. *Mar. Geol.* 340, 57–70. <https://doi.org/10.1016/j.margeo.2013.04.016>
- Dillon, M., Bleil, U., 2006. Rock magnetic signatures in diagenetically altered sediments from the Niger deep-sea fan. *J. Geophys. Res. Solid Earth.* 111(B3). <https://doi.org/10.1029/2004JB003540>
- Dunlop, D. J., 2002. Theory and application of the Day plot (Mrs/Ms versus Hcr/Hc) 2. Application to data for rocks, sediments, and soils. *Journal of Geophysical Research: Solid Earth*, 107(B3), EPM-5. <https://doi.org/10.1029/2001JB000486>.
- Egger, M., Rasigraf, O., Sapart, C.J., Jilbert, T., Jetten, M.S., Röckmann, T., Van der Veen, C., Banda, N., Kartal, B., Ettwig, K.F., Slomp, C.P., 2015. Iron-mediated anaerobic oxidation of methane in brackish coastal sediments. *Environ. Sci. Technol.* 49(1), pp.277-283. <https://doi.org/10.1021/es503663z>
- Elmore, R. D., Engel, M. H., Crawford, L., Nick, K., Imbus, S., Sofer, Z., 1987. Evidence for a relationship between hydrocarbons and authigenic magnetite. *Nature*, 325(6103), 428-430. <https://doi.org/10.1038/325428a0>
- Esteban, L., Enkin, R. J., Hamilton, T., 2008. Gas hydrates and magnetism: Comparative geological settings for diagenetic analysis. *Proceedings of the 6th International Conference on Gas Hydrates* (pp. 1-9).
- Fu, Y., von Dobeneck, T., Franke, C., Heslop, D., and Kasten, S. 2008. Rock magnetic identification and geochemical process models of greigite formation in Quaternary marine sediments from the Gulf of Mexico (IODP Hole U1319A). *Earth Planet. Sci. Lett.* 275, 233-245.
- Gaikwad, V. V., Badesab, F. K., Dewangan, P., Kotha, M., 2021. Diagenesis of Magnetic Minerals in Active/Relict Methane Seep: Constraints from Rock Magnetism and Mineralogical Records from Bay of Bengal. *Front. Earth Sci.* 9, 60. <https://doi.org/10.3389/feart.2021.638594>

- Gaikwad, V., Badesab, F., Kotha, M., 2022. Diagenetic analysis of shallow and deep-seated gas hydrate systems from the Bay of Bengal. *Marine Geology*, 106824. <https://doi.org/10.1016/j.margeo.2022.106824>
- Garming, J. F. L., Bleil, U., and Riedinger, N., 2005. Alteration of magnetic mineralogy at the sulfate-methane transition: analysis of sediments from the Argentine continental slope. *Phys. Earth Planet. Inter.* 151, 290-308. doi: 10.1016/j.pepi.2005.04.001.
- Hirt, A. M., Lowrie, W., Clendenen, W. S., Kligfield, R., 1993. Correlation of strain and the anisotropy of magnetic susceptibility in the Onaping Formation: evidence for a near-circular origin of the Sudbury basin. *Tectonophysics* 225(4), 231–254. [https://doi.org/10.1016/0040-1951\(93\)90300-9](https://doi.org/10.1016/0040-1951(93)90300-9)
- Horng, C.-S., and K.-H. Chen, 2006. Complicated magnetic mineral assemblages in marine sediments offshore of southwestern Taiwan: possible influence of methane flux on the early diagenetic process, *Terr. Atmos. Ocean. Sc.*, 17 (4) 1009-1026.
- Horng, C. S., 2018. Unusual magnetic properties of sedimentary pyrrhotite in methane seepage sediments: Comparison with metamorphic pyrrhotite and sedimentary greigite. *J. Geophys. Res. Solid Earth.* 123(6), 4601-4617. <https://doi.org/10.1002/2017JB015262>
- Housen, B. A., Musgrave, R. J., 1996. Rock-magnetic signature of gas hydrates in accretionary prism sediments. *Earth Planet. Sci. Lett.* 139(3-4), 509–519. [https://doi.org/10.1016/0012-821X\(95\)00245-8](https://doi.org/10.1016/0012-821X(95)00245-8)
- Jiang, W.-T., Horng, C.-S., Roberts, A.P., Peacor, D.R., 2001. Contradictory magnetic polarities in sediments and variable timing of neof ormation of authigenic greigite. *Earth Planet. Sci. Lett.* 193, 1-12. [https://doi.org/10.1016/S0012-821X\(01\)00497-6](https://doi.org/10.1016/S0012-821X(01)00497-6)
- João, H.M., Badesab, F., Gaikwad, V., Kocherla, M. and Deenadayalan, K., 2021. Controls of mass transport deposit and magnetic mineral diagenesis on the sediment magnetic record from the Bay of Bengal. *Marine and Petroleum Geology*, 128, p.104994.
- Johnson, J.E., Phillips, S.C., Clyde, W.C., Giosan, L. and Torres, M.E., 2021. Isolating detrital and diagenetic signals in magnetic susceptibility records from methane-bearing marine sediments. *Geochemistry, Geophysics, Geosystems*, 22(9), p.e2021GC009867.
- Kao, S. J., Horng, C. S., Roberts, A. P., Liu, K. K., 2004. Carbon–sulfur–iron relationships in sedimentary rocks from southwestern Taiwan: influence of geochemical environment on greigite and pyrrhotite formation. *Chem. Geol.* 203(1-2), 153-168. <https://doi.org/10.1016/j.chemgeo.2003.09.007>
- Karlin, R., Lyle, M., Heath, G. R., 1987. Authigenic magnetite formation in suboxic marine sediments. *Nature* 326(6112), 490-493.
- Karlin, R., 1990. Magnetite diagenesis in marine sediments from the Oregon continental margin. *Journal of Geophysical Research: Solid Earth*, 95(B4), 4405-4419. <https://doi.org/10.1029/JB095iB04p04405>
- Kars, M., Kodama, K., 2015. Authigenesis of magnetic minerals in gas hydrate bearing sediments in the Nankai Trough, Offshore Japan. *Geochem., Geophys., Geosys.* 16, 947–961. <https://doi.org/10.1002/2014GC005614>

- Kars, M., Greve, A., Zerbst, L., 2021. Authigenic greigite as an indicator of methane diffusion in gas hydrate-bearing sediments of the Hikurangi Margin, New Zealand. *Front. Earth Sci.* 9, 80. <https://doi.org/10.3389/feart.2021.603363>
- Kulkarni, Y.R., Sangode, S.J., Bloemendal, J., Meshram, D.C. and Suresh, N., 2015. Mineral magnetic characterization of the Godavari River and western Bay of Bengal sediments: Implications to source to sink relations. *Journal of the Geological Society of India*, 85, pp.71-78.
- Larrasoana, J. C., Roberts, A. P., Musgrave, R. J., Gràcia, E., Piñero, E., Vega, M., et al., 2007. Diagenetic formation of greigite and pyrrhotite in gas hydrate marine sedimentary systems. *Earth Planet. Sci. Lett.* 261(3-4), 350–366. <https://doi.org/10.1016/j.epsl.2007.06.032>
- Leslie, B. W., Lund, S. P., Hammond, D. E., 1990. Rock magnetic evidence for the dissolution and authigenic growth of magnetic minerals within anoxic marine sediments of the California continental borderland. *Journal of Geophysical Research: Solid Earth*, 95(B4), 4437-4452. <https://doi.org/10.1029/JB095iB04p04437>
- Lin, Z., Sun, X., Roberts, A.P., Strauss, H., Lu, Y., Yang, X., et al., 2020. A novel authigenic magnetite source for sedimentary magnetization. *Geology*.49(4), 360-365. <https://doi.org/10.1130/G48069.1>
- Lin, Z., Sun, X., Lu, Y., Strauss, H., Xu, L., Gong, J., Teichert, B.M., Lu, R., Lu, H., Sun, W. Peckmann, J., 2017. The enrichment of heavy iron isotopes in authigenic pyrite as a possible indicator of sulfate-driven anaerobic oxidation of methane: Insights from the South China Sea. *Chemical Geology*, 449, 15-29. <https://doi.org/10.1016/j.chemgeo.2016.11.032>
- Liu, J. 2004. High-resolution analysis of early diagenetic effects on magnetic minerals in post-middle-Holocene continental shelf sediments from the Korea Strait. *J. Geophys. Res.* 109:B03103. doi: 10.1029/2003JB002813
- Liu, Q., Roberts, A.P., Torrent, J., Horng, C.S. and Larrasoana, J.C., 2007. What do the HIRM and S-ratio really measure in environmental magnetism?. *Geochemistry, Geophysics, Geosystems*, 8(9).
- Liu, Q., Roberts, A.P., Larrasoana, J.C., Banerjee, S.K., Guyodo, Y., Tauxe, L. and Oldfield, F., 2012. Environmental magnetism: principles and applications. *Reviews of Geophysics*, 50(4).
- Liu, J., Izon, G., Wang, J., Antler, G., Wang, Z., Zhao, J., et al., 2018. Vivianite formation in methane-rich deep-sea sediments from the South China Sea. *Biogeosciences* 15, 6329-6348. doi: 10.5194/bg-15-6329-2018
- Liu, L., Chu, F., Wu, N., Zhang, L., Li, X., Li, H., Li, Z., Zhang, W., Wang, X., 2022. Gas Sources, Migration, and Accumulation Systems: The Shallow Subsurface and Near-Seafloor Gas Hydrate Deposits. *Energies*, 15(19), p.6921. <https://doi.org/10.3390/en15196921>
- Lougheed, B. C., Snowball, I., Moros, M., Kabel, K., Muscheler, R., Virtasalo, J. J., Wacker, L., 2012. Using an independent geochronology based on palaeomagnetic secular variation (PSV) and atmospheric Pb deposition to date Baltic Sea sediments and infer 14C reservoir age. *Quat. Sci. Rev.* 42, 43-58. <https://doi.org/10.1016/j.quascirev.2012.03.013>
- Lovley, D. R., Stolz, J. F., Nord, G. L., Phillips, E. J., 1987. Anaerobic production of magnetite by a dissimilatory iron-reducing microorganism. *Nature* 330(6145), 252-254. <https://doi.org/10.1038/330252a0>

- Mazumdar A., Dewangan P., Peketi A., Gullapalli S., Kalpana M. S., Naik G. P., et al., 2019. The first record of active methane (cold) seep ecosystem associated with shallow methane hydrate from the Indian EEZ. *J. Earth Sys. Sci.* 128:18, <https://doi.org/10.1007/s12040-018-1044-y>
- Mukhopadhyay, G., Mukhopadhyay, S.K., Roychowdhury, M. and Parui, P.K., 2010. Stratigraphic correlation between different Gondwana basins of India. *Journal of the Geological Society of India*, 76, pp.251-266.
- Musgrave, R. J., Bangs, N. L., Larrasoana, J. C., Gràcia, E., Hollamby, J. A., Vega, M. E., 2006. Rise of the base of the gas hydrate zone since the last glacial recorded by rock magnetism. *Geology* 34(2), 117–120. <https://doi.org/10.1130/G22008.1>
- Neretin, L.N., Böttcher, M.E., Jørgensen, B.B., Volkov, I.I., Lüschen, H., Hilgenfeldt, K., 2004. Pyritization processes and greigite formation in the advancing sulfidization front in the Upper Pleistocene sediments of the Black Sea. *Geochimica et Cosmochimica Acta* 68 (9), 2081–2093.
- Özdemir, Ö., Dunlop, D. J., 1997. Effect of crystal defects and internal stress on the domain structure and magnetic properties of magnetite. *Journal of Geophysical Research: Solid Earth*, 102(B9), 20211-20224. <https://doi.org/10.1029/97JB01779>
- Passier, H. D., De Lange, G. J., Dekkers, M. J., 2001. Magnetic properties and geochemistry of the active oxidation front and the youngest sapropel in the eastern Mediterranean Sea. *Geophys. J. Int.* 145(3), 604–614. <https://doi.org/10.1046/j.0956-540x.2001.01394.x>
- Peketi A., Mazumdar A., Sawant B., Manaskanya A., Zatale A., 2022. Biogeochemistry and trophic structure of a cold seep ecosystem, offshore Krishna-Godavari basin (east coast of India). *Mar Pet Geol* 138:105542. <https://doi.org/10.1016/j.marpetgeo.2022.105542>
- Peters, C., Dekkers, M. J., 2003. Selected room temperature magnetic parameters as a function of mineralogy, concentration and grain size. *Phys. Chem. Earth, Parts A/B/C* 28(16-19), 659-667. [https://doi.org/10.1016/S1474-7065\(03\)00120-7](https://doi.org/10.1016/S1474-7065(03)00120-7)
- Petersen, N., Von Dobeneck T., Vali H., 1986. Fossil bacterial magnetite in deep-sea sediments from the South Atlantic Ocean. *Nature* 320, 611–615. <https://doi.org/10.1038/320611a0>
- Philips, S. C., 2018. Diagenetic degradation of paleoenvironmental signals in magnetic susceptibility in the northern Bay of Bengal, *The IRM Quarterly*, Winter 2017-2018, Vol. 27 No.4
- Phillips, S. C., Johnson, J. E., Clyde, W. C., Setera, J. B., Maxbauer, D. P., Severmann, S., Riedinger, N., 2017. Rock magnetic and geochemical evidence for authigenic magnetite formation via iron reduction in coal-bearing sediments offshore Shimokita Peninsula, Japan (IODP Site C0020). *Geochem. Geophys. Geosyst.* 18, 2076–2098. <https://doi.org/10.1002/2017GC006943>
- Prabhakar, K.N., Zutshi, P.L., 1993. Evolution of southern part of Indian East Coast basin. *J. Geol. Soc. Ind.* 41:215–230.
- Ramesh, R., Subramanian, V., 1988, Temporal, spatial and size variation in the sediment transport in the Krishna River basin, India, *J. Hydrol.* 98, 53–65. [https://doi.org/10.1016/0022-1694\(88\)90205-3](https://doi.org/10.1016/0022-1694(88)90205-3)
- Rao, G. N., 2001. Sedimentation, stratigraphy, and petroleum potential of Krishna-Godavari basin, East Coast of India. *AAPGB* 85(9), 1623–1643. <https://doi.org/10.1306/8626CCDF-173B-11D7-8645000102C1865D>

- Rey, D., Mohamed, K.J., Bernabeu, A., Rubio, B., Vilas, F., 2005. Early diagenesis of magnetic minerals in marine transitional environments: geochemical signatures of hydrodynamic forcing. *Mar. Geol.* 215, 215-236. <https://doi.org/10.1016/j.margeo.2004.12.001>
- Reilly, B. T., McCormick, M. L., Brachfeld, S. A., Haley, B. A., 2020. Authigenic ferrimagnetic iron sulfide preservation due to nonsteady state diagenesis: A perspective from Perseverance Drift, Northwestern Weddell Sea. *Geochemistry, Geophysics, Geosystems*, 21(11), e2020GC009380. <https://doi.org/10.1029/2020GC009380>
- Reinholdsson, M., Snowball, I., Zillén, L., Lenz, C., Conley, D.J., 2013. Magnetic enhancement of Baltic Sea sapropels by greigite magnetofossils. *Earth Planet. Sci. Lett.* 366, pp.137-150. <http://dx.doi.org/10.1016/j.epsl.2013.01.029>
- Riedinger, N., Formolo, M. J., Lyons, T. W., Henkel, S., Beck, A., Kasten, S., 2014. An inorganic geochemical argument for coupled anaerobic oxidation of methane and iron reduction in marine sediments. *Geobiology* 12(2), 172-181. <https://doi.org/10.1111/gbi.12077>
- Roberts, A. P., Chang, L., Rowan, C. J., Horng, C. S., Florindo, F., 2011. Magnetic properties of sedimentary greigite (Fe₃S₄): An update. *Rev. Geophys.* 49, RG1002. <https://doi.org/10.1029/2010RG000336>
- Roberts, A. P., 2015. Magnetic mineral diagenesis. *Earth-Sci. Rev.* 151, 1–47. <https://doi.org/10.1016/j.earscirev.2015.09.010>
- Rodelli, D., Jovane, L., Roberts, A. P., Cypriano, J., Abreu, F., & Lins, U., 2018. Fingerprints of partial oxidation of biogenic magnetite from cultivated and natural marine magnetotactic bacteria using synchrotron radiation. *Environmental microbiology reports*, 10(3), 337-343.
- Rodelli, D., Jovane, L., Giorgioni, M., Rego, E. S., Cornaggia, F., Benites, M., et al., 2019. Diagenetic fate of biogenic soft and hard magnetite in chemically stratified sedimentary environments of MamanguáRia, Brazil. *J. Geophys. Res. Solid Earth.* 124 (3), 2313–2330. <https://doi.org/10.1029/2018JB016576>
- Rowan, C. J., Roberts, A. P., 2006. Magnetite dissolution, diachronous greigite formation, and secondary magnetizations from pyrite oxidation: Unravelling complex magnetizations in Neogene marine sediments from New Zealand. *Earth Planet. Sci. Lett.* 241(1-2), 119–137. <https://doi.org/10.1016/j.epsl.2005.10.017>
- Rowan, C. J., Roberts, A. P., Broadbent, T., 2009. Reductive diagenesis, magnetite dissolution, greigite growth and paleomagnetic smoothing in marine sediments: A new view. *Earth Planet. Sci. Lett.* 277(1-2), 223–235. <https://doi.org/10.1016/j.epsl.2008.10.016>
- Sagnotti, L., Roberts, A.P., Weaver, R., Verosub, K.L., Florindo, F., Pike, C.R., Clayton, T., Wilson, G.S., 2005. Apparent magnetic polarity reversals due to remagnetization resulting from late diagenetic growth of greigite from siderite. *Geophys. J. Int.* 160, 89-100. <https://doi.org/10.1111/j.1365-246X.2005.02485.x>
- Sangode, S.J., Suresh, N. and Bagati, T.N., 2001. Godavari source in the Bengal fan sediments: results from magnetic susceptibility dispersal pattern. *Current Science*, pp.660-664.
- Sangode, S.J., Sinha, R., Phartiyal, B., Chauhan, O.S., Mazari, R.K., Bagati, T.N., Suresh, N., Mishra, S., Kumar, R. and Bhattacharjee, P., 2007. Environmental magnetic studies on some

Quaternary sediments of varied depositional settings in the Indian sub-continent. *Quaternary International*, 159(1), pp.102-118.

Sangodkar, N., Gonsalves, M. J., Nazareth, D. R., 2022. Macrofaunal Distribution, Diversity, and Its Ecological Interaction at the Cold Seep Site of Krishna-Godavari Basin, East Coast of India. *Microbial Ecology*, 1-15. <https://doi.org/10.1007/s00248-021-01942-1>

Snowball, I. F., 1991. Magnetic hysteresis properties of greigite (Fe₃S₄) and a new occurrence in Holocene sediments from Swedish Lappland. *Phys. Earth Planet. Inter.* 68(1-2), 32-40. [https://doi.org/10.1016/0031-9201\(91\)90004-2](https://doi.org/10.1016/0031-9201(91)90004-2)

Subramanian, V., 1980. Mineralogical input of suspended matter by Indian rivers into the adjacent areas of the Indian Ocean. *Marine Geology*, 36(3-4), pp.M29-M34.

Suess, E., 2014. Marine cold seeps and their manifestations: geological control, biogeochemical criteria and environmental conditions. *Int. J. Earth Sci.* 103(7), 1889-1916. <https://doi.org/10.1007/s00531-014-1010-0>

Tarduno, J. A., 1995. Superparamagnetism and reduction diagenesis in pelagic sediments: enhancement or depletion? *Geophys. Res. Lett.* 22(11), 1337-1340. <https://doi.org/10.1029/95GL00888>

Treude, T., Krause, S., Maltby, J., Dale, A.W., Coffin, R. and Hamdan, L.J., 2014. Sulfate reduction and methane oxidation activity below the sulfate-methane transition zone in Alaskan Beaufort Sea continental margin sediments: Implications for deep sulfur cycling. *Geochimica et Cosmochimica Acta*, 144, pp.217-237.

Tripathi, R., Kumar, P., Ghosh, S., Nagalingam, J., Singh, H., 2019. Culture based investigations of key microbial functional groups in gas hydrate bearing sediments of the Krishna-Godavari Basin in offshore India. *Marine and Petroleum Geology*, 108, 397-406. <https://doi.org/10.1016/j.marpetgeo.2019.01.034>

Usapkar, A., Dewangan, P., Kocherla, M., Ramprasad, T., Mazumdar, A. and Ramana, M.V., 2014. Enhanced methane flux event and sediment dispersal pattern in the Krishna–Godavari offshore basin: Evidences from rock magnetic techniques. *Marine and petroleum geology*, 58, pp.461-475.

Vigderovich, H., Liang, L., Herut, B., Wang, F., Wurgaft, E., Rubin-Blum, M., Sivan, O., 2019. Evidence for microbial iron reduction in the methanic sediments of the oligotrophic southeastern Mediterranean continental shelf. *Biogeosciences* 16(16), 3165-3181. <https://doi.org/10.5194/bg-16-3165-2019>

Wellsbury, P., Goodman, K., Cragg, B. A., Parkes, R. J., 2000. The geomicrobiology of deep marine sediments from Blake Ridge containing methane hydrate (Sites 994, 995 and 997). In *Proceedings of the Ocean drilling program, Scientific results*, (Vol. 164, pp. 379–391). College Station, TX: Ocean Drilling Program.

Yang, T., Dekkers, M. J., Zhao, X., Petronotis, K. E., Chou, Y. M., 2022. Greigite Formation Modulated by Turbidites and Bioturbation in Deep-Sea Sediments Offshore Sumatra. *Journal of Geophysical Research: Solid Earth*, 127(11), e2022JB024734. <https://doi.org/10.1029/2022JB024734>